QATAR UNIVERSITY

COLLEGE OF ENGINEERING

PARAMETRIC STUDY ON MOMENT REDISTRIBUTION OF FIBER REINFORCED CONCRETE CONTINUOUS BEAMS WITH BASALT FRP BARS

BY

ABDELRAHMAN H. ABUSHANAB

A Thesis Submitted to

the Faculty of the College of Engineering

in Partial Fulfillment of the Requirements for the Degree of

Master of Science in Civil Engineering

June 2019

COMMITTEE PAGE

The members of the Committee approve the Thesis of Abdelrahman H. Abushanab defended on 16/04/2019.

Dr. Wael Alnahhal
Thesis Supervisor

Prof. Khaldoon Bani-Hani
Committee Member

Prof. Antonio Capsoni
Committee Member

Prof. Hisham Eid
Committee Member

Approved:

Abdel Magid Hamouda , Dean, College of Engineering

ABSTRACT

ABUSHANAB, ABDULRAHMAN, H., Masters: June: 2019, Master of Science in Civil Engineering.

Title: Parametric Study on Moment Redistribution of Fiber Reinforced Concrete Continuous Beams with Basalt FRP Bars

Supervisor of Thesis: Wael I. Alnahhal.

The State of Qatar is continuously suffering from the high temperature and humidity which take place most of the year. This can deteriorate and reduce the lifecycle of the reinforced concrete (RC) structures and may increase the possibilities of the corrosion. Recently, composite materials science was developed and produced new non-corrosive composite material like fiber reinforced polymers (FRP). The natural properties of the FRP bars such as low density with high strength, lightweight material, lower lifecycle cost, and corrosion resistance made it preferable reinforcement material in the construction.

Ever since FRP has been used in different concrete elements. However, in continuous beams, the moment redistribution between hogging and sagging sections are still under investigation due to the brittle property of the FRP bars.

The aim of this study is to investigate numerically the impact of using basalt macro fibers (BMF) combined with basalt fiber reinforced polymer (BFRP) bars on the moment redistribution of continuous concrete beams.

The study is focusing mainly on using the finite element analysis (FEA) to investigate the moment redistribution in continuous beams reinforced with BFRP bars. Different FE models were simulated using ABAQUS 6-14 software. They were successfully calibrated using experimental data for flexural testing of continuous RC beams conducted in the Qatar University structural lab. The FE models were verified through

the stress-strain diagrams in which they were matching within the accepted range. The simulated beams were two spans with a size of 200 x 300 x 2000 mm each.

An extensive parametric study was conducted using 144 simulated beams to figure out the key parameters that affect the moment redistribution. The parameters taken into consideration were the BMF volume fraction (0%, 0.75% and 1.5%), stirrups spacing (80 mm, 100 mm and 120 mm), and BFRP bars reinforcement ratio ($0.6\rho_b$, $1.0\rho_b$, $1.8\rho_b$ and $2.8\rho_b$).

In addition, statistical regression analysis was performed using Minitab 17 software to generate a formula for calculating the moment redistribution.

The FE results showed a significant improvement in the moment redistribution when both top and bottom reinforcement are over-reinforced. Also, the results showed that BMFs have positive effect on the moment redistribution. On the other hand, it revealed that there is no significant effects of stirrups spacing on the moment redistribution.

DEDICATION

"To my parents and brothers"

ACKNOWLEDGMENTS

I would like to acknowledge and express my appreciation to all the people who supported me in completing this report. Especially, I express my deep thanks to Dr. Wael Alnahhal who guided me into this study. Finally, I would like to thank the Department of Civil and Architectural Engineering at Qatar University who supported us through this journey of completion of the thesis.

TABLE OF CONTENTS

LIST OF TABLES

LIST OF FIGURES

ABBREVIATIONS

RC	Reinforced Concrete
FRP	Fiber Reinforced Polymer
BMF	Basalt Macro Fiber
BFRP	Basalt Fiber Reinforced Polymer
FEA	Finite Element Analysis
FEM	Finite Element Method
FE	Finite Element
FRC	Fiber Reinforced Concrete
ECC	Engineered Cementitious Composite
CFRP	Carbon Fiber Reinforced Polymer
GFRP	Glass Fiber Reinforced Polymer
CDP	Concrete Damage Plasticity
UTM	Universal Testing Machine
FRC	Fiber Reinforced Concrete
P	Maximum Applied Load
W/C	Water to Cement Ratio

SYMBOLS

δ	Redistribution Coefficient
$f'c$	Concrete Compressive Strength
σ_{t0}	Tensile Failure Stress
d_t	Concrete Tension Damage
ε_t^{pl}	Concrete Plastic Strain in tension
σ_{c0}	Initial Yield Stress
d_c	Concrete Compression Damage
ε_c^{pl}	Concrete Plastic Strain in compression
ν	Poisson's Ratio
φ	Angle of Dialation
ε	Eccentricity
σbo	Initial Biaxial Compressive Stress
σco	Initial Uniaxial Compressive Stress
ρ	Concrete Density
E_c	FRC Modulus of Elasticity
V_f	Chopped Fiber Volume
f_c	Concrete Stress at Any Strain
ε_{cf}	Concrete Strain at f_c Stress
ε_{of}	Maximum Strain at $f'c$
n	Constant Number Contributing the Toughness of the Stress-Strain Curve
β	Shape of Experimental Stress Strain Curve
$f_{c\,lim}$	Stress at 0.96 $f'c$
$\varepsilon_{cf}lim$	Strain at 0.96 $f'c$
r_b	Balanced Reinforcement Ratio

R_A	Actual Reaction
L	Beam Span Length
M_{actual}	Actual Moment
$M_{elastic}$	Elastic Moments
Y	Response Variable
x_n	Predictor Variables
β_n	Regression Coefficients

CHAPTER 1: INTRODUCTION

Reinforced concrete (RC) structures are often subjected to harsh or marine environments during the normal operation of the building. The response of the building under these environments requires full protection against corrosion. Generally, the corrosion can take place when the salts penetrate the member through the cracks with the availability of oxygen and moisture at which it will attach the steel reinforcement and deteriorate the structure. Although, adequate corrosion resistance can be achieved by selecting an appropriate cover to the members; however, the cracks that formulate after the curing period will cause the moisture and oxygen to contact the steel reinforcement, and thereby, the corrosion will attack the steel reinforcement. Traditionally, epoxy coating is applied on the steel reinforcement to resist the corrosion; however, the corrosion could not be fully eliminated. This was the major reason for the drawbacks of using steel reinforcement in the members subjected to the marine environment and replace it with new composite materials like fiber reinforcement polymers (FRP) composites. FRP reinforcement has several advantages such as corrosion resistance, 25% less in weight and ease of manufacture (Cai, Pan, & Zhou, 2017).

FRPs can be used in different applications such as internal reinforcement in new members, strengthening and retrofitting of existing or failure members and also as FRP macro-fibers (Mostafa & Razaqpur, 2017) and (Cai et al., 2017). Previous researches investigated the use of the FRP as internal and strengthening reinforcement for simply supported beams. However, few researchers have studied the behavior of RC continuous beams.

Basalt fiber reinforced polymers (BFRP) is a new type of fiber that is made by melting the igneous rock at 1400 ^{o}c. Basalt fiber can be available in many forms such as bars,

mesh and chopped fiber. It is a nontoxic and environmentally safe material. Previous studied showed that mixing basalt macro-fiber (BMF) with concrete has several advantages such as reducing the crack width, increasing tensile strength, and increasing the concrete rebar bonding. Mixing BMF mini bar with concrete is going smoothly more than other types of fiber due to the higher density that BMF has which is close to the concrete density (Adhikari, 2013) and (Patnaik, Miller, Adhikari, & Standal, 2013). The analysis and design procedure for the FRP members are different than the steel reinforcement due to the difference in the mechanical properties such as young modulus, yielding stress, stress-strain diagram, etc. (Adam, Said, Mahmoud, & Shanour, 2015). The lower young modules that FRPs have cause higher deflection in FRP members compared to the steel member. One solution of this is to use steel stirrups in the FRP reinforced concrete beam (Cai et al., 2017). Bending FRP bars is not recommended because 16 to 75% of the strength will be reduced in the FRP bent bars (Imjai, Guadagnini, & Pilakoutas, 2017).

The most widely approach for designing RC beams is based on assuming the concrete and reinforcement materials will act as elastic material until yielding of the reinforcement. Before yielding, the beam's sections will have constant flexural stiffness. However, the flexural stiffness depends on the cracks and when the cracks form on the member, the member will start acting as a non-linear element. Not all sections will yield and crack at the same time and what exactly happen is the if the section cracks and has sufficient rotational capacity, plastic hinge will be formed, and the moments will be redistributed from low stiffness to high stiffness sections. It allows the members to be more elastic and give a warning before failure. It also helps in reducing the congestion area of rebar in the beam-column connection (Kara & Ashour, 2013). Several standards and design codes provide guidance in redistributing the

moments between hogging and sagging sections in continuous beams reinforced with steel bars. However, most of the design codes and standards are not recommending moment redistribution in continuous beams reinforced with FRP bars (CSA, 2012), (ACI Committee 440, 2015) and (ISIS CANADA, 2007). This is because of the linear elastic behavior of the FRP bars.

The primary focus of this study is to develop and validate a proposed numerical model using the finite element method (FEM) to predict accurately the moment redistribution in fiber reinforced continuous beams reinforced with BFRP bars. The model was simulated using a nonlinear FEM software ABAQUS 6-14. It was verified using previous experimental results obtained from Qatar University structural lab. The model was used to perform an extensive parametric study to investigate the factors that affect the moment redistribution of FRC continuous beams. The studied parameters were BFRP bars reinforcement ratios (0.6ρ_{fb}, 1.0ρ_{fb}, 1.8 ρf_b and 2.8 ρ_{fb}), BMF volume fraction (0%, 0.75% and 1.5%) and stirrups spacing (80 mm, 100 mm and 120 mm).

1.1 Research Significance

Nowadays, Qatar is building major structures in the areas where the water level is high such as Doha Metro, Lusail, Katara, the Pearl, etc. These projects will have a high possibility of deterioration due to the steel corrosion. Therefore, it is the time to replace the steel reinforcement by the non-corrosive FRPs reinforcement. This study has highly beneficial to Qatar because it will help in saving the maintenance cost, increase the projects lifecycle and eliminating the corrosion problem. Also, it will provide a clear picture on the possibility of the moment redistribution in fiber reinforced concrete continuous beams reinforced with BFRP bars.

The success of the project and replacing the steel reinforcement with the non-corrosive BFRP bars will help Qatar a lot in the remaining construction projects.

To the best of the authors' knowledge, this thesis on the moment redistribution of fiber reinforced concrete continuous beams with basalt FRP bars will be the first study to investigate numerically the moment redistribution between the critical sections in fiber reinforced concrete (FRC) continuous beams reinforced with BFRP bars.

1.2 Research Objectives

The principle purpose of the present thesis is to develop a FE model to investigate the impact of replacing the steel reinforcement by BFRP reinforcement in redistributing the moments between hogging and sagging sections in FRC continuous beams reinforced with BFRP bars. The objectives of this study are:

- Developing and verifying a FE model based on a plane stress element that can assist in prediction the moment redistribution in fiber reinforced concrete continuous beams reinforced with BFRP bars.
- Use the developed FE model to perform a parametric study to investigate the effect of different parameters such as BFRP bars reinforcement ratios, BMF volume fractions and stirrups spacings on the flexural strength and moment redistribution.
- Conduct statistical regression analysis to generate a linear model that can predict the moment redistribution in FRC continuous beams reinforced with BFRP bars without performing FE analysis.

1.3 Thesis Organization

This thesis contains seven chapters arranged as the following:

Chapter 1: It includes the introduction, research significance and research objectives.

Chapter 2: It contains a summary of the previous studies related to the topic of this thesis.

Chapter 3: It includes the problem description, finite element modeling procedure and Preliminarily study used to select the mesh size.

Chapter 4: It covers the finite element modeling verification with the experimental data.

Chapter 5: It describes the parametric study conducted in this study

Chapter 6: It includes the results and discussion and the regression analysis of this study.

Chapter 7: It presents summary and conclusions of the study and recommendations for the future work.

CHAPTER 2: LITERATURE REVIEW

Through the past years, the behavior of continuous concrete beams reinforced with steel bars has been investigated in many studies. Nevertheless, few studies were done to investigate the flexural behavior and moment redistribution on continuous concrete beams reinforced with FRP bars. This had led to no recommendation on moment redistribution on RC continuous beams reinforced with FRP bars on the existing design standards (CSA, 2012), (ACI Committee 440, 2015) and (ISIS CANADA, 2007).

In this chapter, a summary of BFRP material characteristics will be reviewed, then the studies that investigated the flexural behavior of FRP beam will be shown. This will be followed by the studies that are investigating the moment redistribution in RC continuous beams reinforced with traditional steel and FRP bars, respectively. Moreover, a FEM verification in previous studies will be shown.

2.1 Material Properties and Characteristics of BFRP Composites

BFRP composites are produced from basalt rocks which are melt at 1400 ^{o}c. In addition, they are non-toxic and considered to be an environmentally safe material. It has high stability and insulation characteristics. BFRP bars have been recently used as an alternative to the steel reinforcement. The fundamental researches to establish design code and guideline is still under investigating, unlike other types of fiber such as carbon and glass fiber. Moreover, they have many advantages such as light-weight and easy handling, high tensile strength, high versatile and increasing the member lifecycle. Compared to the steel reinforcement, BFRP bars have linear elastic behavior with brittle failure, low strain at failure and low modulus of elasticity (High, Seliem, El-Safty, & Rizkalla, 2015).

Chopped fiber can be mixed randomly with the concrete to enhance the shortcomings properties of the concrete such as low tensile strength, brittle failure and wider cracks.

Although the pore structure of the concrete can be improved by using the traditional admixtures such as silica fume. However, the high cost and possibility of concrete shrinkage made researchers to think about an alternative for the traditional admixtures. The first use of fiber reinforced concrete (FRC) was in 1998. Advantages of FRC are their high strength with a high elastic modulus, high thermal stability, chemical stability, good sound insulation and electrical characteristic. It is recommended to use more that 2% chopped fiber to obtain strain hardening behavior of the concrete while, lower than 2% is recommended to be used in the applications where there is requirement of high energy absorption, spalling and fatigue, impact resistance, and fracture toughness of the concrete (Ayub, Shafiq, & Nuruddin, 2014).

(Ayub et al., 2014) conducted experimental tests on 12 specimens with 73 to 85 MPa compressive strength and 0 to 3% BMF. The aim of the study was to investigate the mechanical properties of the FRC such as compressive strength (both cubes and cylinders), splitting tensile strength, and the flexural strength. The compressive strength for the three samples was not affected more than ± 4% compared to the average compressive strength. The strain capacity was significantly increased by 4.76%, 9.99 and 12.2% for 1%, 2% and 3%, BMF, respectively. Concrete Post peak behavior in the stress-strain diagram improved by adding the BMF. In addition, the tensile splitting strength significantly increased by increasing the BMF and the average increase for the 3 groups were 1.64%, 5.27%, and 23.95% for 1%, 2% and 3% BMF, respectively. The flexural behavior increased considerably by 18.15%, 36.12% and 27.17% for 1%, 2% and 3% BMF, respectively. The reduction on the flexural strength for the 3% BMF specimen took place due to the extra water demand needed for this group.

2.2 Flexural Performance of Simply Supported RC Beams Reinforced with FRP Bars

(Cai et al., 2017) carried out a study on 18 beams with different compression strengths, tension strains, tension strengths and longitudinal BFRP reinforcement ratios. The objective of their study was to investigate the flexural behavior of BFRP engineered cementitious composite (ECC) beams. It was found that the ultimate strength of the beams increases linearly with increasing all variables except the tension strength of ECC which caused 1.5% increment in the ultimate strength. In addition, it was found that the ultimate deflection increases with increasing the compressive strength and tension strain of ECC and had no relation with the ultimate stress. Moreover, increasing the reinforcement ratio had changed the failure mode and had decreased the ultimate strength.

(Adam et al., 2015) carried out a parametric study on 10 beams to investigate the flexural behavior of concrete beams reinforced with glass FRP bars. The parameters used in this study were the reinforcement ratio and compressive strength. The test results showed that with increasing the reinforcement ratio, the crack width and the mid-span deflection were significantly decreasing and when the reinforcement ratio increased to 270%, the ultimate load increased to 97%. When the compressive strength increased to 45 MPa and 70 MPa, the cracking width decreased to 52%, and 80%, respectively.

(Pawłowski & Szumigała, 2015) carried out a parametric study on 30 beams to study the flexural behavior of BFRP beams with different reinforcement ratios. It was shown that the reinforcement ratio has an effect on the flexural strength and the failure mode. Also, it is shown that the deflection increased with decreasing of the reinforcement ratio, while the ultimate loads and stiffness increased with increasing the reinforcement ratio.

2.3 Performance of Continuous Beams Reinforced with Steel Bars

Many researchers investigated the parameters that affect the performance and the moment redistribution of continuous beams reinforced with steel bars. It is worthy to mention that the first study on the moment redistribution was conducted by Glanville and Thomas in 1935 as reported by (Park, Park, & Paulay, 1975). In the following sections, different parameters affecting the maximum curvature, ductility, moment redistribution will be discussed.

2.3.1 Reinforcement Ratio

The reinforcement ratio parameter started with (Park et al., 1975). (Park et al., 1975) studied the relation between the moment-curvature and reinforcement ratios for both compressive and tensile failure modes. The study was concluded that the maximum curvature for the compressive failure beams decreased due to the ductility lost in these beams. However, this was not the case for the tensile failure beams. On the effect of reinforcement ratios, it was concluded that increasing the compressive reinforcement can improve the maximum curvature, while increasing the tensile reinforcement will decrease the maximum curvature.

(Lin & Chien, 2000) studied the effect of different reinforcement ratios on the moment redistribution of RC continuous beams reinforced with steel reinforcement. The study aimed to obtain a formula to calculate the moment redistribution. They showed that the ductility and moment redistribution can be effectively active by increasing bottom reinforcement and decreasing top reinforcement.

2.3.2 Concrete Compressive Strength

(Lopes & Bernardo, 2003) studied the plastic rotation on high strength concrete beams. The objective of their study was to verify if the high strength concrete can provide the ductility of the structure. They concluded that plastic tendency of the beams increases

with increasing the concrete compressive strength because the neutral axis decreases at failure as the compressive strength increases.

2.3.3 Sample Size

(Carpinteri, Corrado, Paggi, & Mancini, 2009) simulated a model to study the sample size effect on the ductility of the reinforced concrete elements. They concluded that the beams behavior tends to be more brittle with increasing the beams depth.

2.3.4 Moment Redistribution

(Ernst, 1958) studied the moments and forces distribution after the first yielding in continuous beams. He concluded that all beams have the same behavior in moments and forces distribution.

(Kodur & Campbell, 1996) conducted a nonlinear FE analysis on a continuous prestressed concrete beam. The aim of their study was to investigate the beams moments redistribution. They have derived several conclusions about the moment redistribution such as moment redistribution can be increased with increasing the beam stiffness, moment redistribution can be decreased with increasing the neutral axis depth to effective depth (c/d) at the support section, moment redistribution decreases when the span length to effective thickness (l/d) is increasing.

(Jędrzejczak & Knauff, 2002) conducted a study on moment distribution between the critical sections. They showed the moment redistribution depends on the order of the cracks and not necessary to move from hogging to sagging sections.

(Do Carmo & Lopes, 2006) have investigated analytically the parameters that affect the moment redistribution on continuous beams reinforced with traditional steel reinforcement. The parameters studied are the structural type, type of load, compressive strength, and slenderness of the beam. It was concluded that higher plastic rotation can be achieved by higher compressive strength. Plastic rotation for the concentrated load

is less than the uniformly distributed load. Beams that have two-spans have less plastic-rotation than the higher number of spans. The plastic rotation increases with higher span to depth ratio.

(Piotr & Krzysztof, 2017) conducted an experimental study to investigate the moment redistribution on continuous beams reinforced with steel bars, they concluded that the direction of the moment is not constant, and some beams experienced an inverse moment redistribution.

(Bagge, O'Connor, Elfgren, & Pedersen, 2014) conducted an experimental study on 12 beams. The objective of the study was to investigate the influence of longitudinal and transverse reinforcement ratios, and the concrete strength on the continuous beams reinforced with steel bars. They concluded that increasing the tensile reinforcement will cause a reduction in moment redistribution and may redistribute the moment before steel yielding. However, the transverse reinforcement did not show a significant effect on the studied beams. Moreover, they concluded that increasing concrete strength can increase the moment redistribution.

2.3.5 Design Codes for Moment Redistribution

Euro code (EN, 2004) stated the condition in which the rotation angle in the concrete sections can be ignored. To implement this, the redistribution coefficient δ shall be:

$\delta > 0.44 + 1.25 \frac{x}{d}$ for $f'c \leq 50MPa$

$\delta > 0.56 + 1.33 \frac{x}{d}$ for $f'c \geq 50MPa$

Where:

δ is the ratio between the redistributed bending moment to linear elastic bending moment which is equal to $\frac{M_{redistributed}}{M_{linear\ elastic}}$. $\frac{X}{d}$ is the relative height of the compressive zone.

Standards such as (EN, 2004) and (ACI 318-08) are allowing to use linear elastic analysis with limited moment redistribution at ultimate limit state. The allowable

moment redistribution is different from code to another; in Eurocode and Canadian standards, moment redistribution is a function of the ratio of the compressive strength to effective depth $\frac{X}{d}$, but in American code, it function of the strain in the tensile reinforcement in which $\varepsilon_{.t} \geq 0.0075$, Eurocode is limiting the moment redistribution up to 30% while it is limited to 20% in the American and Canadian standards.

2.4 Behavior of Continuous Beams Reinforced with FRP bars

As shown in the previous section, continuous beams can redistribute the forces between the critical sections due to ductility property of the steel which is not applicable in the FRP reinforcement, i.e., FRP reinforcement stress-strain relationship is linear up to failure, which is the reason of not recommending moment redistribution in design codes and standards of FRP beams.

(Tezuka, Ochiai, Tottori, & Sato, 1995) did an experimental and numerical work on RC beams reinforced by FRP or steel bars or pretensioned wire. The aim of their study was to determine the moment redistribution in RC continuous beams. The beams length was 4400 mm with a cross section of 120 x 200 mm. The parameters used in this study were reinforcement type such as Aramid FRP, Glass FRP, steel prestressing wire. The outcomes of this study were: the moment redistribution obtained from the AFRP and CFRP beams were 14.1% and 29.7%, respectively.

(Grace, Soliman, Abdel-Sayed, & Saleh, 1998) conducted an experimental study to investigate the performance and elasticity of RC beams reinforced with FRP and steel bars. The reinforcement type used were steel, carbon fiber reinforced polymers (CFRP), and glass fiber reinforced polymers (GFRP). They concluded that by using GFRP transverse reinforcement, the shear deformation and deflection will increase. In addition, using GFRP stirrups will change the failure mode from flexural failure to shear failure or flexural shear failure. In general, it was found that the beams that are

reinforced with FRP are experiencing more deflection than the than beams that are reinforced with steel reinforcement.

(Razaqpur & Mostofinejad, 1999) conducted an experimental study on the shear behavior of continuous beams reinforced with CFRP and steel shear reinforcement. The objective of the study was to test the ability to use FRP material in the transverse reinforcement. They concluded that CFRP reinforcement has the same performance of steel reinforcement in shear behavior. Moreover, they found that 80% of the beam's strength has been retained when over-reinforcement is used which means that FRP bars may have some ductility in this condition.

(Habeeb & Ashour, 2008) investigated the flexural behavior of continuous beams reinforced with steel or GFRP bars and steel stirrups. For the beams that have top reinforcement ratio less than bottom reinforcement ratio, moment redistribution was observed. The beams which were reinforced with GFRP reinforcement have wider cracks than the beams reinforced with steel reinforcement. The load capacity was not significantly affected by increasing the top reinforcement. However, it was improved with increasing the bottom reinforcement. The deflection values were compared against the equations established in (ACI Committee 440, 2015) and a good agreement was obtained in the comparison.

(Gravina & Smith, 2008) investigated analytically the moment redistribution and cracks in continuous beams reinforced with FRP and steel bars. The parameters studied were steel with different ductility type, CFRP and GFRP bars, ribbed or grain FRP bars. Top and bottom sections were reinforced with the same amount of reinforcements. The effect of grain FRP type was negligible which is an indication of the independence between load and the bond. However, the beams which reinforced with grain coated bars experienced fewer cracks than the ribbed reinforcement. The moment's ratio

between the two sections was slightly increased then stopped in FRP beam; hence, in the steel beams, it was not stopped due to steel ductility. FRP beams experienced more deflection than the steel beams which resulted in more rotational capacity.

(El-Mogy, El-Ragaby, & El-Salakawy, 2010) investigated the flexural behavior of continuous concrete beams reinforced with FRP bars. Four beams with a dimension of 200 x 300 mm over two spans each span is 2800 mm have been tested. The parameters studied were reinforcement type and the longitudinal reinforcement ratios. Two beams reinforced with GFRP, one with CFRP, and one with steel reinforcement for comparison purpose. The study outcomes were increasing GFRP at the mid-span will decrease the mid-span displacement. It was observed also that moment was redistributed in the steel beams before yielding. For the GFRP and CFRP beams, it was found that 23% and 42% of the moment were transferred to mid-span sections, respectively. In the second beam where it was reinforced with GFRP, top reinforcement ratio was increased which caused inverse moment redistribution. They concluded that designing a beam with 20% moment redistribution will not affect the performance in service and ultimate states.

(El-Mogy, El-Ragaby, & El-Salakawy, 2011) published an article discussing the effect of transverse reinforcement on flexural behavior of continuous concrete beams reinforced with FRP bars. Seven beams have been investigated up to failure. Six of them were reinforced with GFRP as longitudinal reinforcement, while one was reinforced with steel reinforcement. The beams have a dimension of 200 x 300 mm over two spans each is 2800 mm. GFRP and steel bars were used in transverse reinforcement. All beams were designed for 20% moment redistribution. It was shown that the beams have moment redistribution values from 23% to 33%. It was observed

also that the moment redistribution can be improved by decreasing the transverse reinforcement spacing.

(Kara & Ashour, 2013) conducted an experimental study on RC continuous beam reinforced by FRP reinforcement to study the moment redistribution. They concluded that the failure for under-reinforced FRP sections was sudden and there was no possibility of moment redistribution. On the other hand, over-reinforced sections experienced the same failure, but with higher curvature at failure.

(Lou, Lopes, & Lopes, 2015) conducted a study to investigate the effect of neutral axis depth on the moment redistribution. The FRP types used are GFRP and CFRP. The position of neutral axis before cracking was not changed and the change of curvature with the change of neutral axis is negligible. However, after cracking, the neutral axis depth decreased and tended to stabilize with stabilization of cracks and the change of neutral axis with the curvature was started very fast and then slowed down. This movement depends on the elastic modulus and ductile characteristic of the reinforcement. Steel beams were slower than FRP beams before yielding and much faster after yielding. The moment started to redistribute when the first crack occurred in the middle support. GFRP beams experienced higher moment redistribution than the CFRP beams.

(Rahman, Mahmoud, & El-Salakawy, 2016) conducted an experimental study to investigate the performance of the continuous RC beams reinforced with GFRP and steel bars. Seven T-beams were studied. It was noticed from the tests that prior to first cracking load, the end reaction is equal to the elastic theory reaction. The beam reinforced with steel bars experienced 17.1% moment redistribution before yielding. After the steel yielded, the moment redistribution was decreased to 10.1% at the failure load. The beams which were designed not to redistribute the moments resulted in 4.8

to 5.7% moment redistribution at the failure load. The beams which were designed to have 15% moment redistribution resulted in 7.2 to 15.2 % moment redistribution at the design load and 8.2 to 23.3% moment redistribution at the failure load. They have concluded that more lateral reinforcement in the flange will increase the flexural stiffness of the sagging section and will increase the moment redistribution. They showed also, the transverse reinforcement effect on the moment redistribution.

(Rahman, Mahmoud, & El-Salakawy, 2017) investigated the unsymmetrical loading on moment redistribution in RC continuous beams reinforced by GFRP reinforcement. Six beams had been studied up to failure. Three loading conditions were considered. The First condition, loading both spans equally, the second condition, loading both spans with a ratio of 1.5 and the third condition, loading one span only. The beams tested under symmetrical load exhibited a higher percentage of moment redistribution than the same beams tested under 1.5 loading ratio. This is because of the high crack at the middle support under symmetrical loading condition. In the case of unsymmetrical loading, the high load span had less crack width, strain, and deflection. The beams with one load only experienced similar behavior of symmetrically loaded beams.

2.4.1 Design Codes for Moment Redistribution in FRP beams

Flexural design formulas can be found in Canadian code (CSA, 2012) and American code (ACI Committee 440, 2015). However, they are not allowing for moment redistribution in FRP beams.

2.5 Finite Element Modeling Verification.

(Cai et al., 2017) carried out a nonlinear finite element model using ATENA software to study the flexural behavior of the beams reinforced with steel and BFRB bars. In their model, concrete was designed as quasi-brittle and both cracks and crash will be under tension and compression loads. Concrete cracking and crushing were simulated

by employing the rankine failure criterion and Menetrey-Willam failure. The steel and BFRP bars were modeled as discrete reinforcing bars in the form of truss element and 1D reinforcement material. The bond between the concrete and BFRP was incorporated due to the brittle effect of the concrete. To validate the model, four beams were tested experimentally and compared with the FE model. The comparison was in terms of the ultimate load, loads versus deflection and failure mode. The load capacities gave a maximum ratio of 1.06.

(Adam et al., 2015) carried out a nonlinear FEM by the nonlinear software ANSYS. A comparison to validate the model was done between experimental results and FE model in terms of ultimate loads, first cracking load and maximum deflection. The crack locations and directions that was predicted by ANSYS met with the experimental results.

The cracking loads and ultimate strength values from ANSYS and from the experimental results were close, the crack loads ratio vary between 0.82 to 1.16, and the ultimate strength ratio vary between from 0.81 to 1.06.

(Mostafa & Razaqpur, 2017) carried out a nonlinear finite element model for the FRP-retrofitted beams in flexure using the nonlinear software LS-DYNA. The study was to predict the debonding load, shear stresses, and strain after verifying the model. A comparison to validate the model was done between test results and the FE model in terms of delamination loads and mid-span deflection. The delamination load ratios varies from 0.89 to 1.16 and the mid-span deflection ratios values vary from 0.76 to 1.73.

(Pawłowski & Szumigała, 2015) carried out a nonlinear FE model by the nonlinear software ABAQUS to study the failure mechanism, deflection, and ductility of a simply supported beam. The applied loads were in displacement control mode with a

displacement rate of 1.0 mm/min. Concrete damaged plasticity (CDP) was assumed for the concrete which is based on brittle-plastic degradation model. Linear elastic isotropic material was assumed for BFRP reinforcement while the steel reinforcement was assumed as linear elastic isotropic. The reinforcements were modeled as 2-nodes truss elements embedded in 4-nodes element of plane stress. A comparison to validate the model was done between test results and FE model in terms of load-midspan deflection curves and the predicted values agree with experimental values.

(Metwally, 2017) carried out a nonlinear FE model to simulate deep beams reinforced with GFRP bars. The objective of the study was to investigate the failure mechanism, deflection, and ductility of a simply supported beam. In the FE model, concrete was modeled by CDP. GFRP reinforcement was simulated as elastic isotropic 1D material until failure using 3D 2 nodes first order truss elements. All the elements in the model have the same size of the mesh to ensure that any material shares the same node. Full bond was assumed between GFRP and the concrete. The FE model was verified using load-deflection response. It showed that the FE model gives stiffer results than the experimental results because of the micro-crack which shown in the lab and neglected in the software. The mean ratio of the experimental diagonal crack to the numerical model is 0.99. Failure mode was accurately predicted and it was matching the experimental results.

CHAPTER 3: FINITE ELEMENT MODELING PROCEDURES

In this study, the objective was to generate a FE model that simulates all characteristics of FRC beam reinforced with BFRP bars. The model was employed to perform a parametric study to study the effect of different parameters on the moment redistribution of continuous beams reinforced with BFRP bars using the ABAQUS 6-14 nonlinear FE software. The modeling procedures used in this study is reported in the following sections. The results obtained by the FE model was compared with the experimental results which were collected from Qatar University lab as it will be shown in Chapter 4.

3.1 Model Description

All the modeled beams have a rectangular cross section of 200 x 300 mm with a total length of 4000 mm and clear span of 3600 mm. The beams were modeled as a continuous beam over two spans each one is 1800 mm. The loading was simulated as an equal concentrated load at the middle of each span. BFRP reinforcement was simulated for the flexural reinforcement, while regular steel was simulated for the transverse reinforcement. The FRC was modeled by merging BMF properties in the concrete properties. The geometry and dimension of the simulated beams are shown in Figure 1.

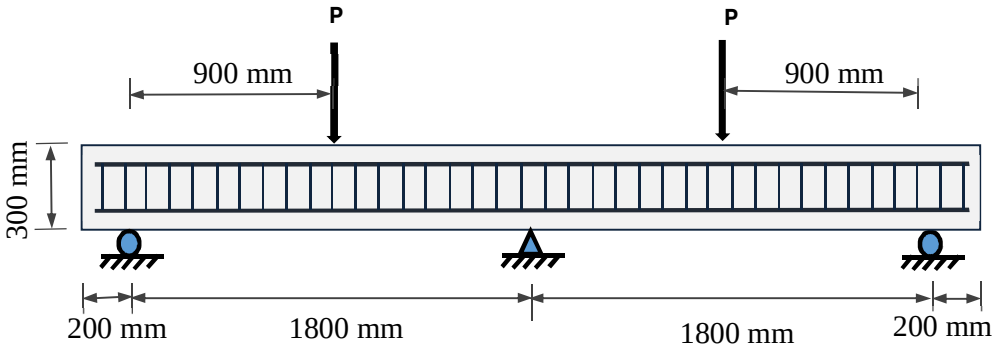

Figure 1: Geometry and dimensions of modeled beams

3.2 Problem Description

The equivalent elastic shear force and bending moment diagrams for the modeled beams which are continuous over two spans and loaded at each mid-span with a value of P kN are shown in Figure 2.

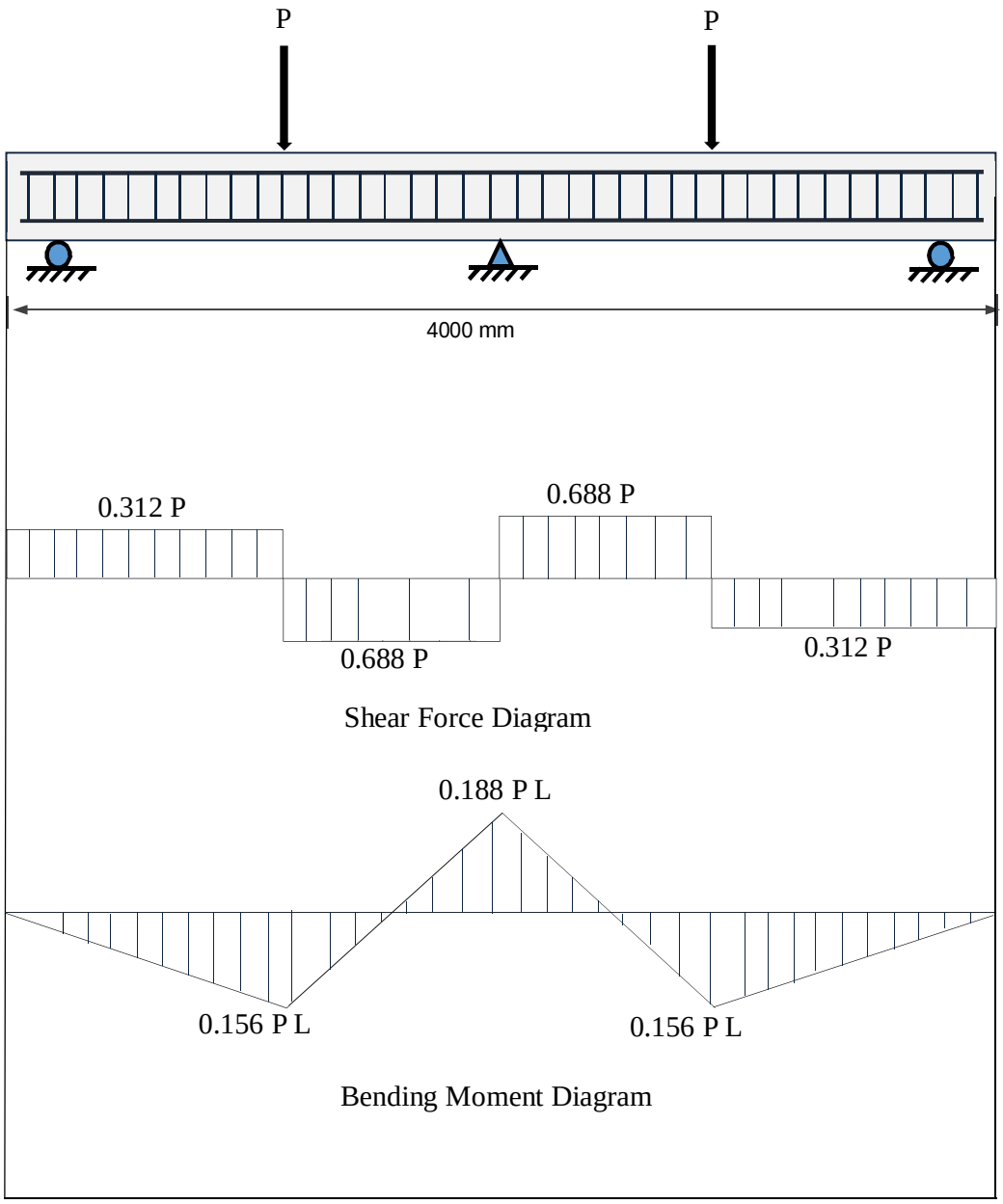

Figure 2: Elastic bending moment and shear force diagrams for the modeled beams

As shown in Figure 2, the moment at the hogging section is higher than the moment at the sagging section. However, when the beam is loaded and the first crack occurred, the moments between hogging and sagging sections will start to redistribute from the lower stiffness section to the higher stiffness section as shown in Figure 3.

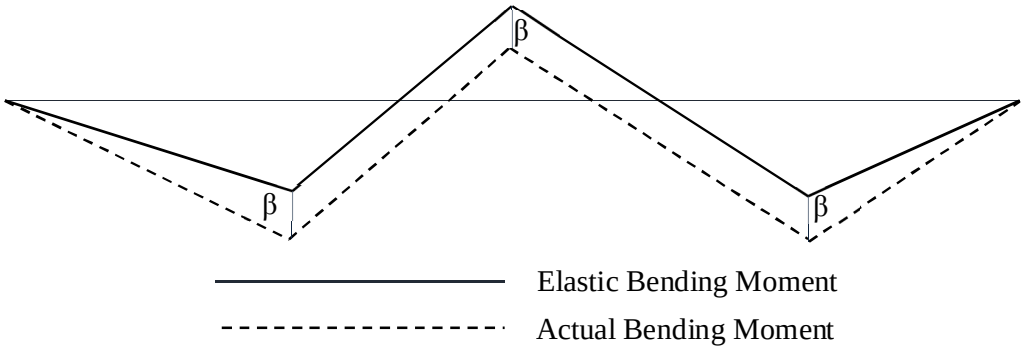

Figure 3: Elastic and actual bending moment diagram for the modeled beams

The redistribution procedures are available in the design codes for the RC beams reinforced with steel bars, but it is still under investigation for the beams that are reinforced with FRP bars because of the brittle material property of the FRP bars.

3.3 Materials Modeling

3.3.1 Concrete Element

FRC was modeled using two dimensional four nodes solid and homogeneous element. Concrete Damage Plasticity (CDP) provided by ABAQUS 6-14 was adopted to model the concrete. The nonlinear behavior was simulated using the stress-strain relationship governed by equation 3. The concrete compressive strength $(f'c)$ used in this model was equal to 50 GPa for all modeled beams. The properties of CDP model are that it can represent the inelastic behavior of concrete. Moreover, it is applicable for plain and reinforced members. In addition, it can model the monotonic, cyclic and dynamic loading, and it allows for the stiffness recovery effects at the loading stage. The two main failure conditions for this model are compressive crushing and tensile cracking (Abaqus 6-14).

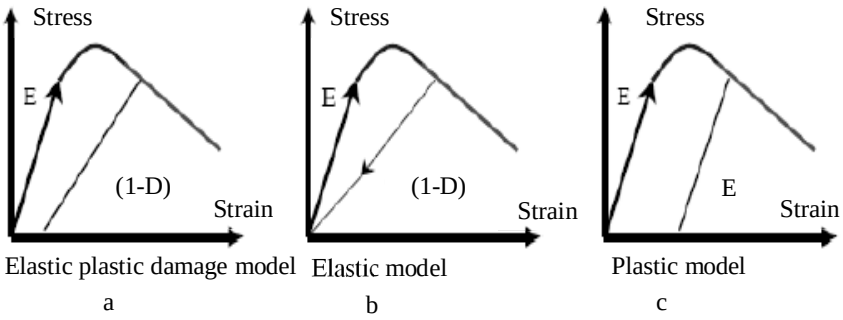

Figure 4: Concrete unloading response at different stages (Jason, Pijaudier-Cabot, Huerta, & Ghavamian, 2004)

Figure 4 shows the concrete unloading response of a) elastic plastic damage, b) elastic and c) plastic models. A shown in 4b, we can see the zero stress is corresponding to zero strain, which is underestimating the damage. On the other hand, when elastic plastic relation is used, the unloading curve will follow the elastic slope which represents an overestimated value of strain as shown in the Figure 6c. However, the CDP model combines the previous two behavior and it captures the actual unloading curve as shown in Figure 6a (Jason et al., 2004)

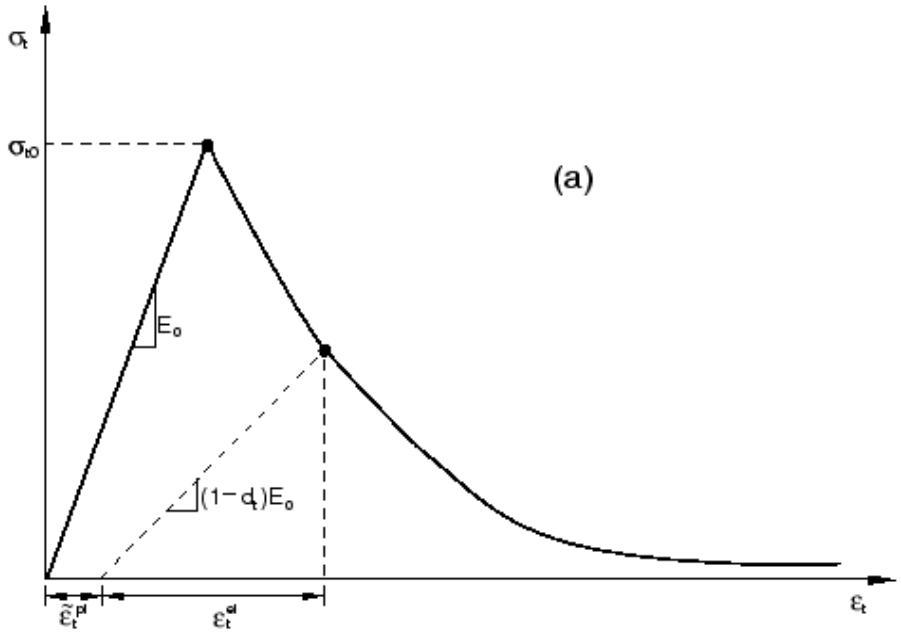

Figure 5: Concrete response to uniaxial loading in tension (Systèmes, 2013)

As presented in Figure 5, the concrete tensile response will follow a linear elastic relation until the stress is reached to the failure stress, σ_{t0}. After this point, the elastic stress strain relationship will be converted to stress versus inelastic strain. At the inelastic region, if the concrete specimen is unloaded, the unloading response will be affected by the tension damage, d_t causing plastic strain, ε_t^{pl}. The damage parameter has a value from zero to one in which zero represents no damage and 1 represents a full damage.

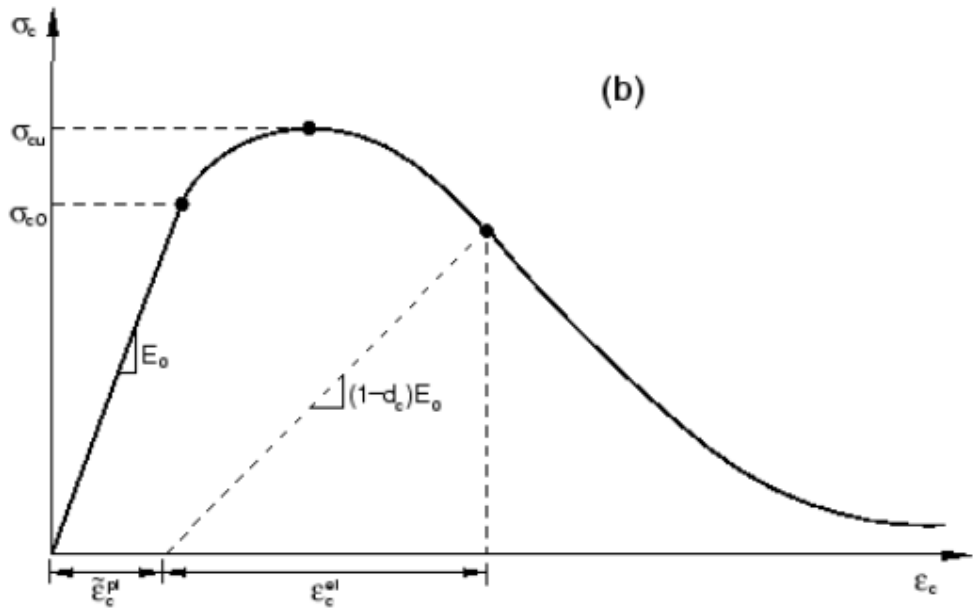

Figure 6: Concrete response to uniaxial loading in compression (Systèmes, 2013)

As shown in Figure 6, the compression stress-strain diagram will follow a linear elastic relation until the stress is reached to the initial yield stress, σ_{c0}. After this point, the stress strain relationship will be converted to stress versus inelastic strain. At the inelastic curve, if the concrete specimen is unloaded, the unloading response will be affected by the compression damage, d_c causing plastic strain, ε_c^{pl}. The damage parameter has a value from zero to one in which zero represents no damage and 1 represents a full damage. In both tension and compression, the CDP assumes the reduction of the initial modulus of elasticity is governed by:

$E=(1-d)E_o$. (1)

Where, d is the damage parameter and E_o is the initial modulus of elasticity.

The parameters that need to be defined in plasticity CDP are:

1. Poisson's ratio ν which control the volume change for the inelastic behavior. In this study, ν was assumed to be 0.18.
2. Angle of dilation φ which control the plastic strain developed during plastic shearing. In this study, the default value of 20 was assumed.

3. Eccentricity ε which is the eccentricity of the plastic potential surface with default value of 0.1. In this study, the default value was used.
4. The ratio of initial biaxial compressive to initial uniaxial compressive yield stress, σbo/ σco with default value of 1.16. In this study, the defult value was used.
5. The ratio of second tensile stress to compressive stress K_c with a default value of 0.67. In this study, the defult value was used.
6. Concrete density ρ which was assumed to be 2.5 $\frac{kN}{m3}$.
7. Modulus of Elasticity E_c:

   In this model, the following formula is used to calculate modulus of elasticity E_c

   $E_c = \left(10300 - 400\, V_f\right)\sqrt[3]{f'c}$ $(in\ MPa)$ (Ayub, Khan, & Shafiq, 2018) (2)

   Where:

   V_f is the chopped fiber volume used.

   f'c is concrete compressive strength.

8. Stress-Strain Curves:

   FRC stress-strain compressive curve consists of two curves: the ascending branch and the descending branch. The ascending branch can be predicted using the following equation (Ayub et al., 2018) ;

   $$f_c = \frac{n\beta f'_c(\frac{\varepsilon_{cf}}{\varepsilon_{of}})}{n\beta - 1 + (\frac{\varepsilon_{cf}}{\varepsilon_{of}})^{n\beta}} \quad (in\ MPa) \qquad (3)$$

   Where:

   f_c= concrete stress at any strain (in MPa).

   ε_{cf}= concrete strain at stress f_c.

   ε_{of}=maximum strain at f'_c.

   n= constant contributing the toughness of the stress strain curve.

β= depends on the shape of experimental stress strain curve and can be calculated as the following:

For control specimens: $\beta = \left(\frac{f'c}{65.23}\right)^3 + 2.59$ (Ayub et al., 2018) (4)

For FRC specimens: $\beta = \frac{1}{\left(1-\left(\frac{E_{cf}}{E_{it}}\right)\right)}$ (Ayub et al., 2018) (5)

3.3.2 Reinforcement Material

In this study, longitudinal and transverse reinforcements were modeled using a one dimensional, two nodes truss element. Truss element has been selected because it is carrying only axial load and it has only one degree of freedom, i.e., displacement occurred in the direction of the axial load only. Truss element can simulate the nonlinearity and plastic deformation of the reinforcement. The concrete interaction with the reinforcement was modeled as an embedded region constraint. Figure 7 shows truss degree of freedom in 3D.

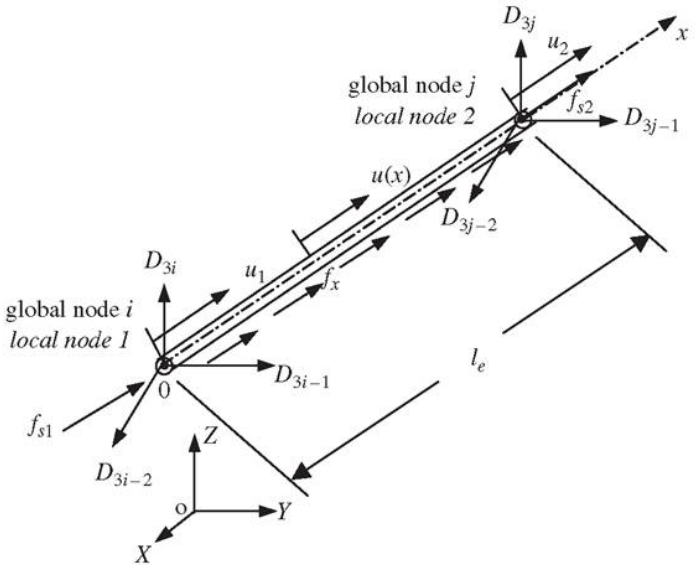

Figure 7: Truss element used in reinforcement modeling

1. Steel Reinforcement

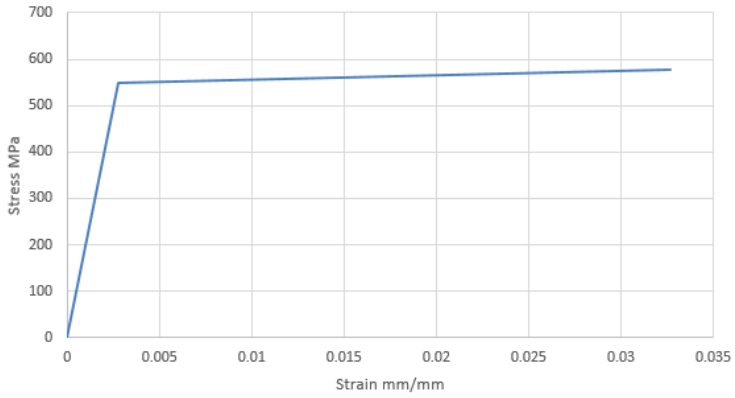

Figure 8: Stress-strain relationship for steel reinforcement material

Steel reinforcement was modeled as an isotropic elastic perfectly plastic stress-strain relationship as shown in Figure 8. The elastic part is defined using the modulus of elasticity and poisson's ratio, while the plastic part is defined using the yield stress and the inelastic strain. Steel reinforcement was used for all stirrup's reinforcement. The mechanical properties of the used steel reinforcement are presented in Table 1.

Table 1: Mechanical Properties of Steel Reinforcement

Property	Value
Poisson's Ratio	0.3
Modulus of Elasticity (GPa)	195
Yield Strain	0.027
Yield Stress (MPa)	520
Ultimate Stress (MPa)	660

2. BFRP Reinforcement

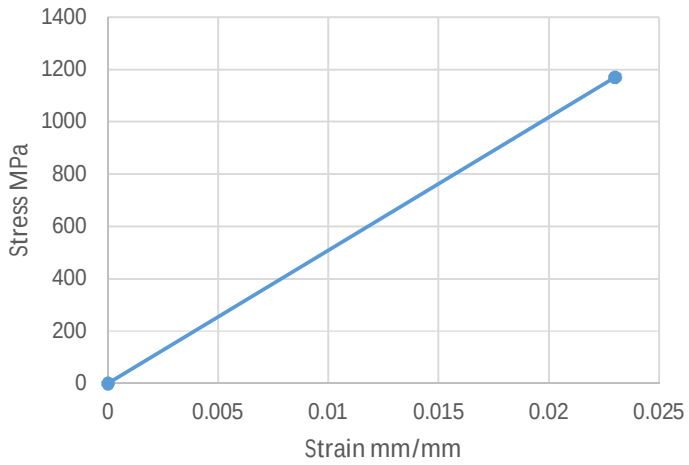

Figure 9: Stress-strain relationship for BFRP reinforcement material

BFRP reinforcement was modeled as an elastic linear material up to failure as shown in Figure 9. The mechanical properties of the used BFRP bars are presented in Table 2.

Table 2: Mechanical Properties of BFRP Bars

Property	Value
Poisson's Ratio	0.18
Modulus of Elasticity (GPa)	50
Ultimate Stress (MPa)	1170
Ultimate Strain	0.023

3.4 Geometric Modeling

Displacement controlled method with a dynamic explicit form was carried out to investigate the studied beams in the FE software ABAQUS 6-14. The beams were modeled as 2D 4 nodes elements. The model was converged at a mesh size of 30 mm. Reinforcement area was modeled by multiplying the actual quantity by the element area. Perfect bond was assumed between the concrete and the reinforcement. To avoid any stress concentration under the load, 50 mm under the load was modeled as a rigid material with a modulus of elasticity = 90 GPa as shown in the brown color in Figure 10. The method of loading was chosen to be enforcing the vertical displacement at a

rate of 1 mm/step up to failure. The applied load (P) and displacement values were continually measured at each step.

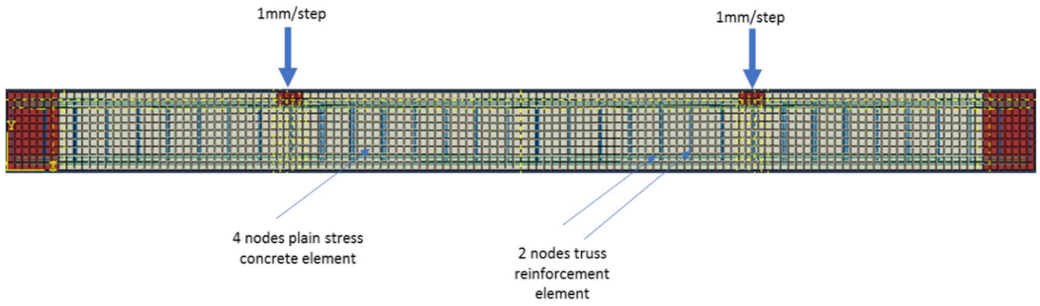

Figure 10: 2D view of the modeled beams

As shown in Figure 10, three nodes were added at the supports set. Two for roller supports and one for the pin support at the middle. The pin support was designed to have 2 degrees of freedom, while the roller support was designed to have 1 degree of freedom. In addition, two nodes were added for the loading set at the top mid-span of each beam. The displacement was measured by adding two nodes in the bottom of each mid-span which will act as strain gauges.

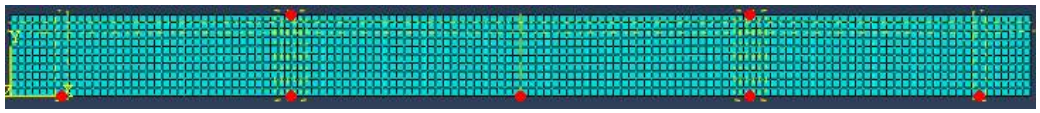

Figure 11: Simulated locations of supports, loading sets and strain gauges

Sensitivity study was conducted to select the optimal mesh size for the model. Trials were conducted on one beam using different mesh sizes. The selected range of mesh was from 10 mm to 50 mm. The selected beam was R2R3 which has 4 φ 10 in the top and 6 φ 10 in the bottom. The suitable mesh is the mesh which has high accuracy with

less nodes and less computational time. So, 30 mm mesh was selected in this model. The results of the mesh trials are shown in Figure 12.

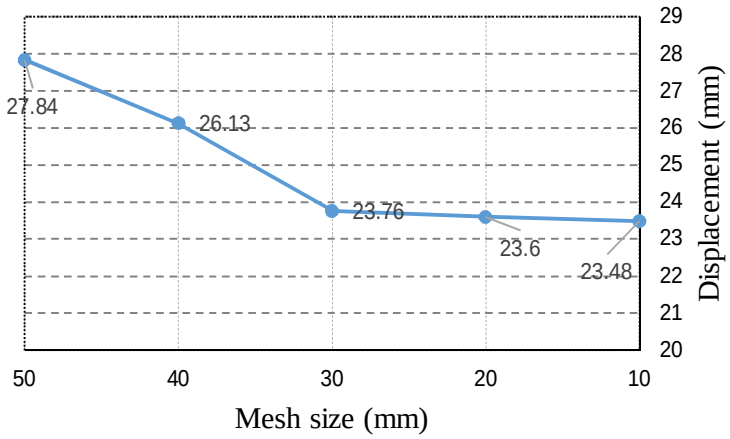

Figure 12: Mesh sizes sensitivity study

CHAPTER 4: FINITE ELEMENT MODEL VERIFICATION

Finite element modeling scheme shown in Chapter 3 can be verified by comparing the results obtained by the FE model against the experimental results of FRC continuous beams obtained from Qatar University lab. In this chapter, experimental results will be used to verify the accuracy of the proposed FE model.

4.1 Experimental Works

A total of 5 beams had been tested at the Qatar University structural lab. The beams were loaded at five-points with a loading span of 1800 mm. The beams were designed to have a flexural failure by maintaining the minimum stirrups spacing governed by the design code. The minimum spacing required to maintain a flexural failure is 120 mm (d/2). All beams had a cross section of 200 x 300 mm and were continuous over two spans with a total length of 4000 mm and clear span of 3600 mm. The beams were loaded as a displacement control loading using the universal testing machine (UTM). The deflections at each mid-span were reported using LVDT. Strain gauges were used to measure the strain in concrete and steel (See Figure 13).

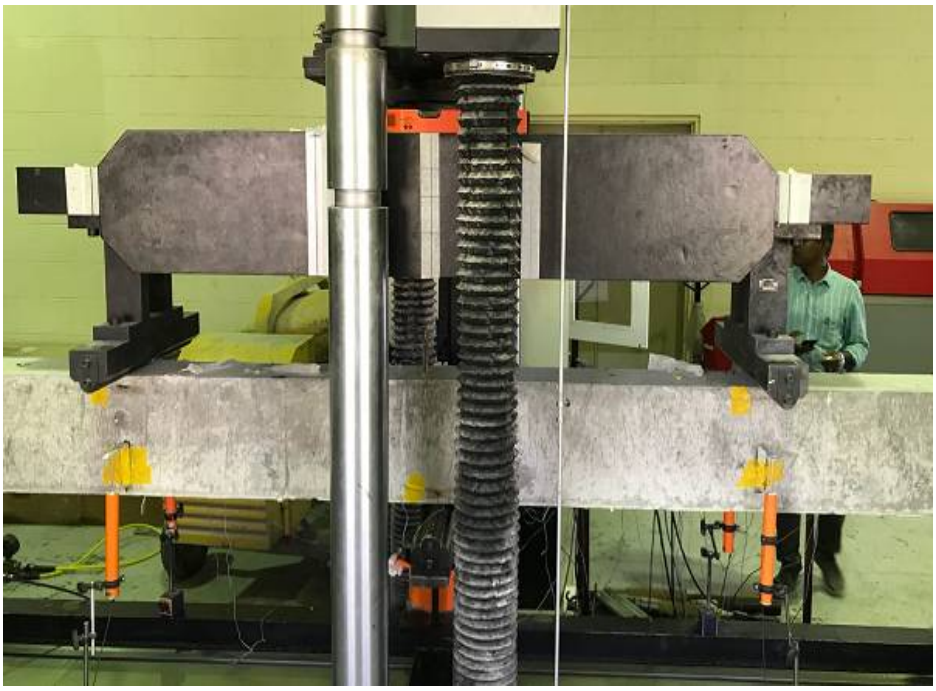

Figure 13: Tested beams at Structural Lab. at Qatar University

The clear cover used in the experiment was 30 mm for all beams with 25 mm spacing between longitudinal reinforcement. The spacing between the transverse reinforcement was varying from 80 mm to 120 mm, while all stirrups had been chosen to be 10 mm diameter. The longitudinal reinforcement had three types, steel, BFRP ribbed bars and BFRP sand coated bars. The volume of fraction of BMF used in this experiment was varying from 0% to 1.5%. Table 3 shows the testing matrix of the tested beams.

Table 3: Testing Matrix of the Tested Beams

Beam No.	Bottom Reinforcement	Top Reinforcement	Stirrups Spacing (mm)	%BMF	Longitudinal Reinforcement
1	6 ϕ 10	4 ϕ 10	120	0	BFRP-Ribbed Bar
2	6 ϕ 10	4 ϕ 10	120	0.75	BFRP-Ribbed Bar
3	4 ϕ 10	6 ϕ 10	120	0.75	BFRP-Ribbed Bar
4	4 ϕ 12	3 ϕ 12	120	0.75	Steel
5	6 ϕ 10	4 ϕ 10	120	1.5	BFRP-Ribbed Bar

For the verification purpose, all beams were chosen. Beam 1 was selected to verify the BFRP reinforcement bars. Beam 2 and 3 were selected to verify the different ratios of longitudinal reinforcement and BMF. Beam 4 was selected to verify the steel reinforcement. Beam 5 was selected to verify the steel reinforcement and different ratios of BMF. The comparison was in terms of load-displacement diagram for the numerical model and the experimental results.

4.2 Stress-Strain Verification

To validate the compressive stress-strain relation in equation 3, the predicted curve was compared with the experimental values for fiber percentages of 0%, 0.75% and 1.5%, respectively.

The results obtained for the 0% FRC with $f'c$ =39.39 MPa are summarized Figure 14.

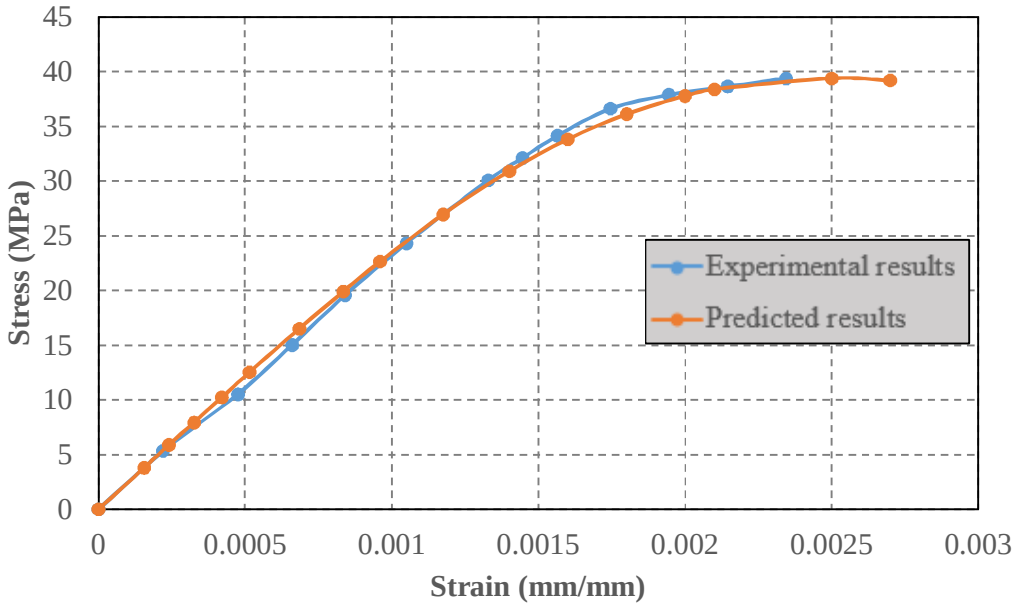

Figure 14: Experimental and predicted stress-strain diagram for 0% FRC

As shown in Figure 14, good agreement was achieved between the experimental and the predicted FRC stress-strain curve governed by equation 3.

The same analysis was done on the 0.75% FRC samples. The predicted stress-strain curves were drawn and checked with the experimental curve as shown in Figure 15.

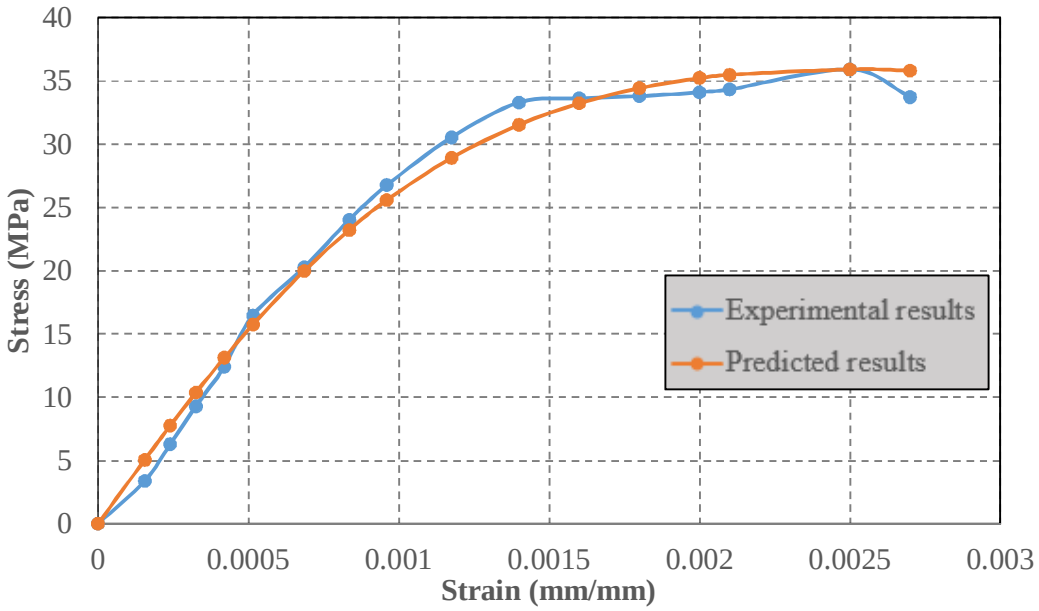

Figure 15: Experimental and predicted stress-strain diagram for 0.75% FRC

From Figure 15, the two curves are matching with good agreement. The same formula was used for the samples of 1.5% FRC and the results obtained are shown in Figure 16.

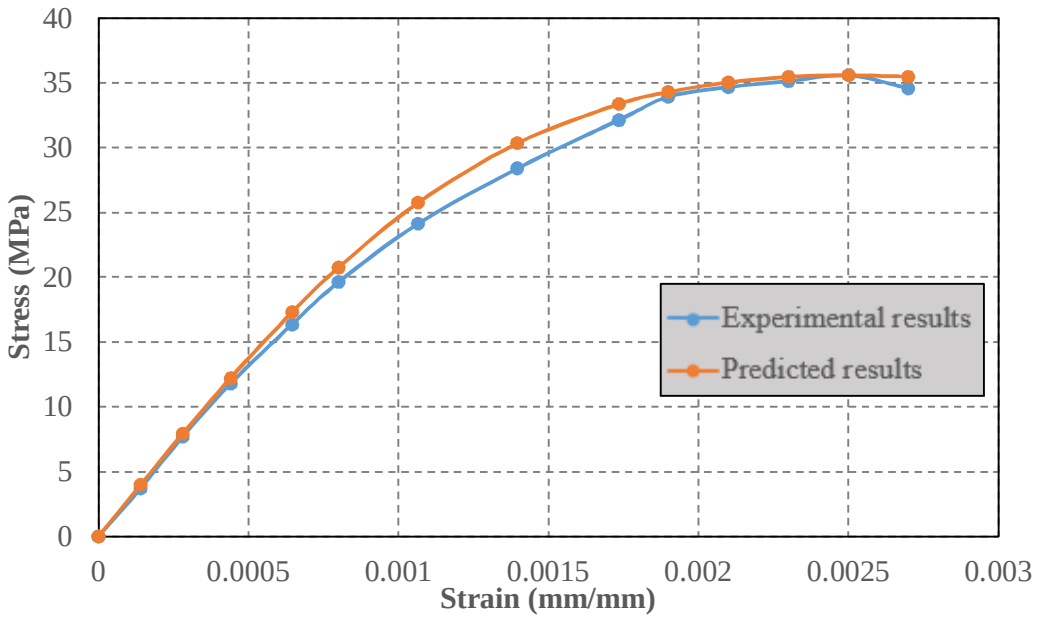

Figure 16: Experimental and predicted stress-strain diagram for 1.5% FRC

From Figure 16, there is a good matching between stress-strain curves between the prediction value and the lab results.

For the descending branch the following formula was used (Ayub & Khan, 2017):

$$f_c = f_{c\,lim} x \exp\left(1 - n + 0.1\, {v_f}^2\right) x \left(\frac{\varepsilon_{cf}}{\varepsilon_{of}} - \frac{\varepsilon_{cf}lim}{\varepsilon_{of}}\right)^{(1-0.1 v_f)} \quad (6)$$

Where:

$f_{c\,lim}$ and $\varepsilon_{cf}\,lim$ are the stress and strain at 0.96 $f'c$, respectively.

For the tensile behavior in this study, trial and error were used to obtain the optimum model.

4.3 Load-Displacement Diagram Verification

As discussed in section 4.1, beams 1, 4, 5, 6 and 10 were chosen for FE verification. The reaction forces and mid-span deflection values have been calculated at each step of the analysis. Load-displacement diagrams have been plotted for the five beams and compared with the experimental results. The chosen beams are summarized in Table 4

Table 4: Selected Beams for Load-Displacement Diagram Verification with the Experimental Results

Beam No.	Bottom Reinforcement	Top Reinforcement	Stirrups Spacing (mm)	%BMF	Longitudinal Reinforcement
1	6 ϕ 10	4 ϕ 10	120	0	BFRP-Ribbed Bar
2	6 ϕ 10	4 ϕ 10	120	0.75	BFRP-Ribbed Bar
3	4 ϕ 10	6 ϕ 10	120	0.75	BFRP-Ribbed Bar
4	4 ϕ 12	3 ϕ 12	120	0.75	Steel
5	6 ϕ 10	4 ϕ 10	120	1.5	BFRP-Ribbed Bar

The comparison between the experimental and FE model load-displacement diagrams at the mid-span is shown in Figure 17.

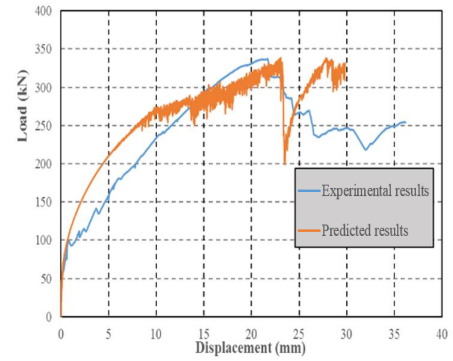

a) Beam #

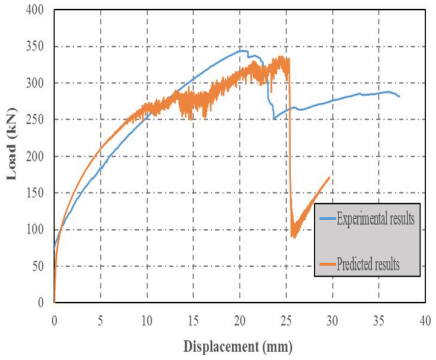

b) Beam #

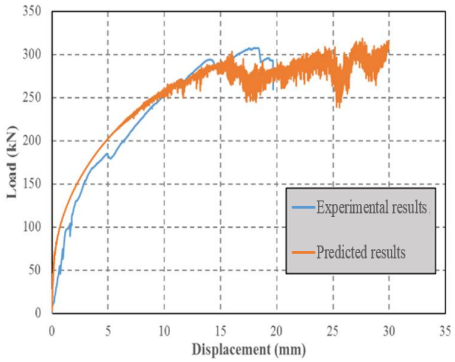

c) Beam #

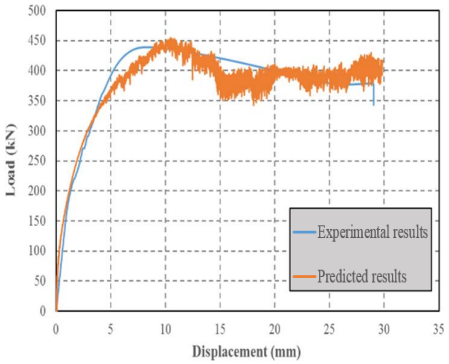

d) Beam #

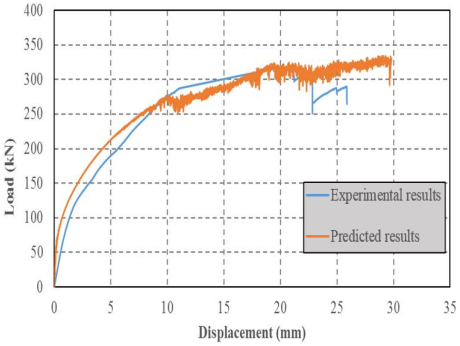

e) Beam #

Figure 17: Experimental and predicted load-displacement diagrams for all beams

Another verification for the P values in Figure 17 can be done using the analytical equations provided by (ACI 318-08) for beam 4 and (Rjoub, 2006). The P values can be calculated using equation 15 while the nominal moments can be calculated using equation 16-18:

$$P = \frac{2(2\,x\,M^{+}+M^{-})}{L} \quad (7)$$

$$M_{nc} = A_s f_y \left(d - \frac{a}{2}\right) \quad (8)$$

$$M_{nf} = \frac{\Delta FTS \times b \times h^2}{6} \quad (9)$$

$$M_{n,total} = M_{nc} + M_{nf} \quad (10)$$

The results obtained from these analytical are summarized in Table 5

Table 5: Actual Versus Predicted P Values

Beam #	Predicted P (kN)	Actual P (kN)	Actual/ Predicted P
1	335	344	1.03
2	337	344	1.02
3	316	308	0.97
4	441	450	1.02
5	360	351	0.98

From Figure 17, it is shown that the predicted load-displacement curves are stiffer than the experimental curves. The reason behind this higher stiffness in FE model is due to the microcracks in the concrete which is not included in the FE model. For all beams, there is good agreement in the predicted and measured load-displacement diagrams. The maximum ratio of experimental-to-predicted ultimate load was 1.03. On the other hand, the maximum ratio of experimental-to-predicted displacement was 1.09. This indicates that the FE model which is used for FRC and BFRP bars can capture all the

behavior of continuous FRC beams reinforced with BFRP bars. The drop in predicted curve in 17a and 17b is due to the higher number of bottom reinforcement which is arranged in two layer, three bars in each layer, in which if one fail, the remaining will continue in carrying the load.

CHAPTER 5: PARAMETRIC STUDY

The main objective of conducting the parametric study is to investigate the effect of different parameters on the flexural strength and moment redistribution of a continuous beam reinforced with BFRP bars. The main parameters taken into consideration were the BFRP bars reinforcement ratios, volume fraction of BMF and stirrups spacing. The parametric study was used also to conduct statistical regression analysis to generate a linear model that can predict the moment redistribution percentages of the beams reinforced with BFRP bars without performing FE analysis. Every investigated parameter was changed to cover a wider range that was not studied experimentally or analytically.

5.1 Longitudinal Reinforcement Ratios

The balanced reinforcement ratio for the FRP bar can be calculated as per (ACI Committee 440, 2015):

$$\rho_{fb} = 0.85\,\beta_1 \frac{fc'}{f_{fu}} \frac{E_f \varepsilon_{cu}}{E_f \varepsilon_{cu} + \varepsilon_{fu}} \tag{11}$$

Also, it can be calculated as per (CSA, 2012):

$$\rho_{fb} = \frac{\alpha_1 \beta_1 fc'}{E_{frp} \varepsilon_{frpu}} x \frac{0.0035}{(0.0035 + \varepsilon_{frpu})} \tag{12}$$

The balanced reinforcement ratios were 0.002605 and 0.002183 as per (ACI Committee 440, 2015) and (CSA, 2012), respectively. The parametric study was chosen based on the reinforcement ratio as under-reinforcement, balance-reinforcement and over-reinforcement ratios. 4 levels of reinforcement were selected to monitor the behavior of the continuous beams. The studied levels have reinforcement ration starting from 0.6 ρ_{fb} to 2.8 ρ_{fb} as shown in the Table 6.

Table 6: Reinforcement Configuration of Simulated Beams

Code	Reinforcement	ρ_{fb}	ρ_f / ρ_{fb} (ACI440.1-15)	ρ_f / ρ_{fb} (S806-12)
R0	2 ϕ 8	0.00167	0.640	0.593
R1	2 ϕ 10	0.00262	1.005	0.930
R2	4 ϕ 10	0.00523	2.009	1.860
R3	6 ϕ 10	0.00760	3.013	2.791

A matrix was set to have a combination of these 4 levels of reinforcement ratios as shown in Table 7

Table 7: Matrix of the Simulated Beams

Top Reinforcement	Bottom Reinforcement			
	R0	R1	R2	R3
R0	R0R0	R0R1	R0R2	R0R3
R1	R1R0	R1R1	R1R2	R1R3
R2	R2R0	R2R1	R2R2	R2R3
R3	R3R0	R3R1	R3R2	R3R3

As shown in Table 7, the matrix has a combination of 16 beams. The matrix will be repeated for each investigated variable of stirrups spacing and volume fraction of BMF.

5.2 Stirrups Spacing (SS)

The stirrups chosen for all beams were steel stirrups with a diameter of 10 mm. Flexural behavior is governed by using ϕ 10 @ 120 mm. The stirrups spacing was changing, while the diameter was kept 10 mm to separate the effect of stirrups spacing. In this study, three levels of spacing were used as follow (80 mm, 100 mm and 120 mm).

5.3 Basalt Macro Fiber (BMF) Percentages

Three volume fractions of BMF were chosen to be studied as follow (0%, 0.75% and 1.5%).

The matrix shown in Table 6 which consist of 16 beams was repeated for each investigated parameter of stirrups spacing and volume fraction of BMF. So, a total of 144 (16 x 3 x 3) beams were modeled and the results are presented in Chapter 6.

CHAPTER 6: RESULTS AND DISCUSSIONS

The results obtained from the parametric study are presented and discussed throughout this chapter. As previously mentioned, 144 FRC continuous beams over two spans were numerically modeled using ABAQUS 6-14 software. The displacement and end reaction values were recorded in every loading step. The three main effects to be examined in this study are the volume of fraction of BMF, BFRP reinforcement ratios, and the stirrups spacing. All the modeled beams were designed to have a flexural failure by maintaining the minimum transverse reinforcement spacing. The results showed 117 beams failed in compression by concrete crushing while 27 failed in tension by BFRP rupture. The beams that failed in tension were the group with the following reinforcement R2R0, R3R0 and R3R1.

6.1 Ultimate Flexural Strength

The effect of three parameters namely, volume of fraction of BMF, stirrups spacing, and bottom longitudinal reinforcement ratios on the maximum applied load (P) was investigated. The first two parameters were studied as a combination to investigate if there is an effect of combining both parameters on the (P) values, while the third parameter was studied individually.

6.2 Effect of BMF and Stirrups Spacing

In this section, three different BMF volume fractions were investigated: 0%, 0.75% and 1.5%. Also, three stirrups spacing were used: 80 mm, 100 mm and 120 mm. The effect of these two parameters on the (P) values was studied by dividing the model into sets based on the top reinforcement. Each set has a specific top reinforcement namely, R0, R1, R2 and R3, and different values for other parameters.

6.2.1 Top Reinforcement (R0)

The set that has R0 as top reinforcement was the first set being modeled. This set was modeled with 2 ϕ 8 BFRP bars as the top longitudinal reinforcement, while it has different values of the other parameters. A total of 36 were modeled in this set as shown in Table 8:

Table 8: Testing Matrix for R0 Set

Beam No.	*Bottom Reinforcement*	*Top Reinforcement*	*%BMF*	*Stirrups Spacing (mm)*
R0R0	*2 ϕ 8*	*2 ϕ 8*	*0*	*80*
			0.75	*100*
			1.5	*120*
R0R1	*2 ϕ 10*	*2 ϕ 8*	*0*	*80*
			0.75	*100*
			1.5	*120*
R0R2	*4 ϕ 10*	*2 ϕ 8*	*0*	*80*
			0.75	*100*
			1.5	*120*
R0R3	*6 ϕ 10*	*2 ϕ 8*	*0*	*80*
			0.75	*100*
			1.5	*120*

BMF and stirrups spacing effect on the maximum applied load is shown in Figure 18. In this Figure, it is clear to see that the addition of BMF with different volume fractions did not contribute in enhancing the (P) values for all the beams regardless of the stirrups spacing. Also, it is shown that there was no clear trend for the relation between (P) values with the BMF and stirrups spacing. The conclusion confirmed that the BMF and stirrups spacing have no effect on (P) when the top reinforcement ratio = 0.6 ρ_{fb}. The main role of the stirrups is to resist the shear forces. On the other hand, BMF main role is to enhance the concrete behavior such as reducing the crack width. This is the reason behind not getting a significant effect on (p) with different values of stirrups spacing and BMF.

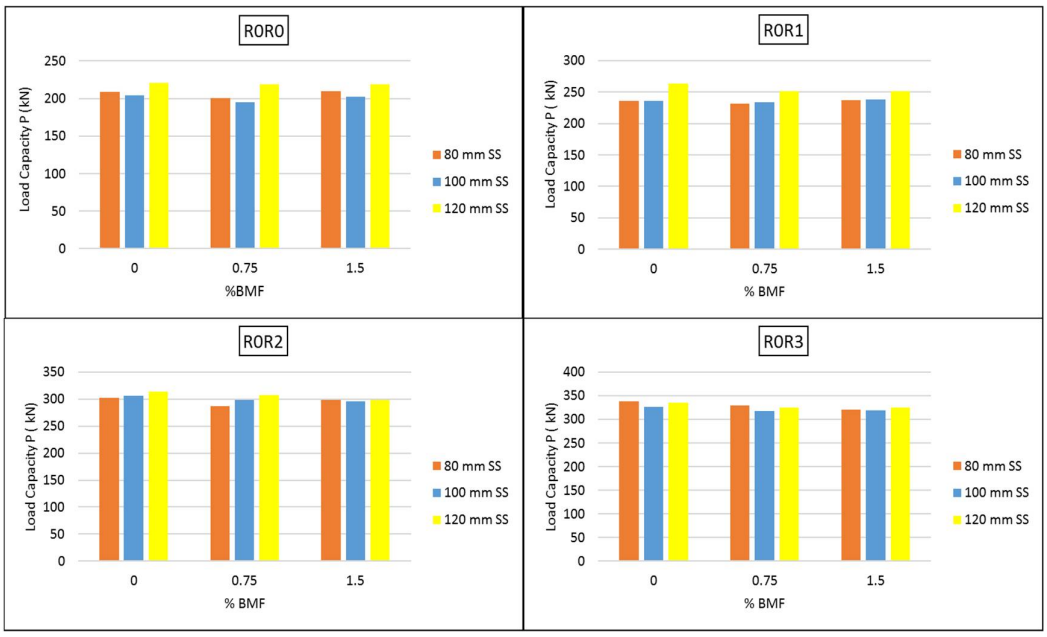

Figure 18: Load capacity for different stirrups spacing and BMF percentages for R0 group

6.2.2 Top Reinforcement (R1)

A similar analysis was conducted on the set that has R1 as top reinforcement. The modeled beams in this set are shown in Table 9.

Table 9: Testing Matrix for R1 Set

Beam No.	Bottom Reinforcement	Top Reinforcement	%BMF	Stirrups Spacing (mm)
R1R0	2 ϕ 8	2 ϕ 10	0	80
			0.75	100
			1.5	120
R1R1	2 ϕ 10	2 ϕ 10	0	80
			0.75	100
			1.5	120
R1R2	4 ϕ 10	2 ϕ 10	0	80
			0.75	100
			1.5	120
R1R3	6 ϕ 10	2 ϕ 10	0	80
			0.75	100
			1.5	120

As shown in Figure 19, similar results to R0 set were observed.

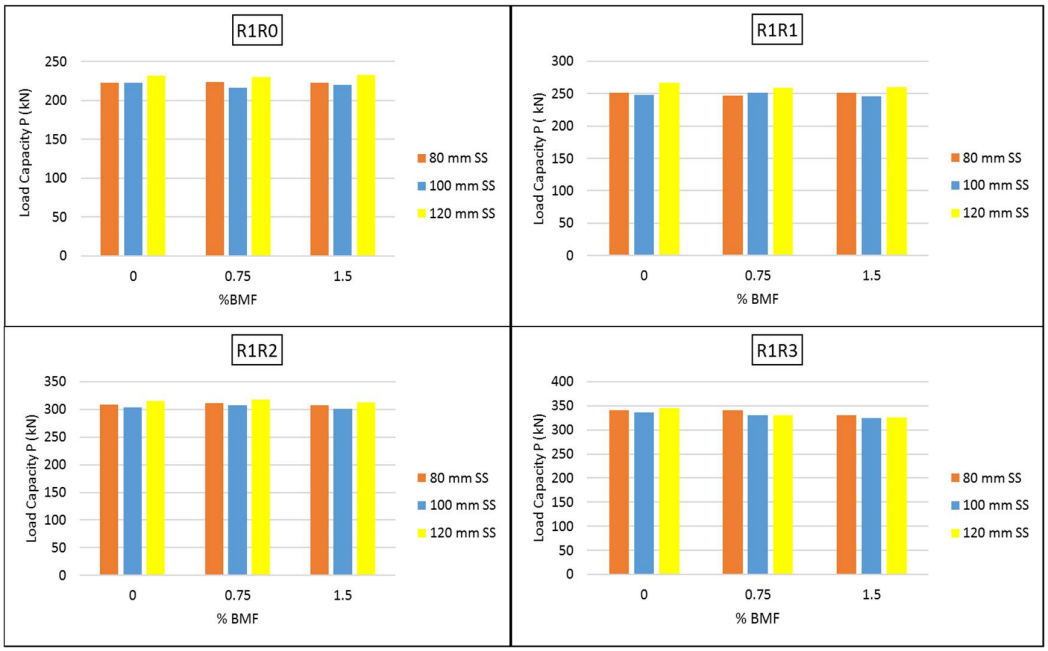

Figure 19: Load capacity for different stirrups spacing and BMF percentages for R1 group

6.2.3 Top Reinforcement (R2)

The set that has R2 as top reinforcement were modeled with the similar concept of R0 set. The modeled beams in this set are shown in Table 10.

Table 10: Testing Matrix for R2 Set

Beam No.	Bottom Reinforcement	Top Reinforcement	%BMF	Stirrups Spacing (mm)
R2R0	4 ϕ 10	2 ϕ 10	0	80
			0.75	100
			1.5	120
R2R1	4 ϕ 10	2 ϕ 10	0	80
			0.75	100
			1.5	120
R2R2	4 ϕ 10	2 ϕ 10	0	80
			0.75	100
			1.5	120
R2R3	6 ϕ 10	2 ϕ 10	0	80
			0.75	100
			1.5	120

Figure 20 presents the results to R0 set. It can be shown that there is no relation between stirrups spacing and BMF with the P values regardless of the longitudinal reinforcement.

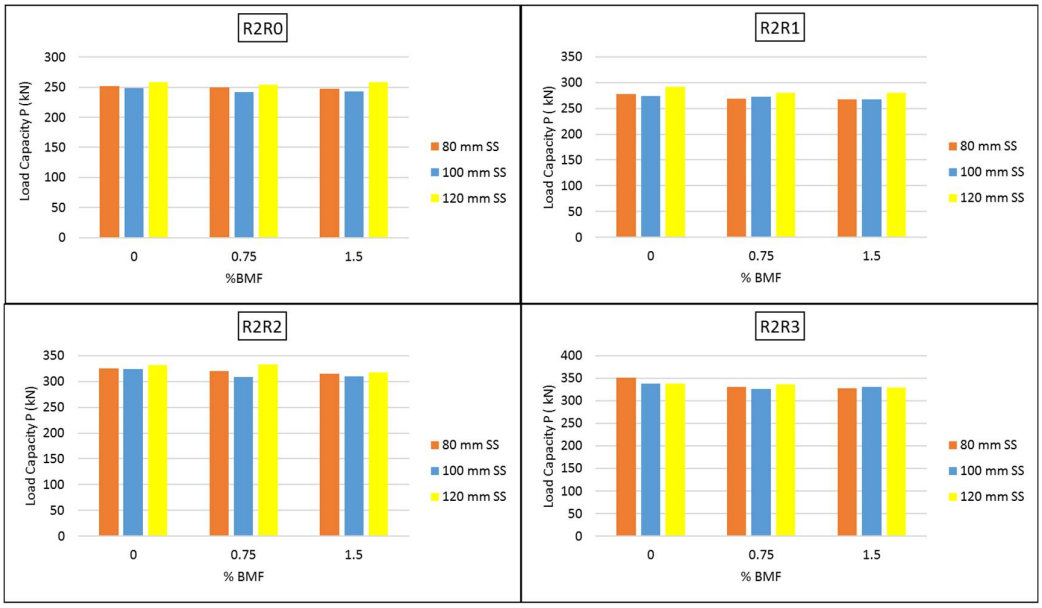

Figure 20: Load capacity for different stirrups spacing and BMF percentages for R2 group

6.2.4 Top Reinforcement (R3)

The set that has R3 as top reinforcement was modeled with the similar concept of R0 set. The modeled beams in this set are shown in Table 11.

Table 11: Testing Matrix for R3 Set

Beam No.	Bottom Reinforcement	Top Reinforcement	%BMF	Stirrups Spacing (mm)
R3R0	4 ϕ 10	6 ϕ 10	0	80
			0.75	100
			1.5	120
R3R1	4 ϕ 10	6 ϕ 10	0	80
			0.75	100
			1.5	120
R3R2	4 ϕ 10	6 ϕ 10	0	80
			0.75	100
			1.5	120
R3R3	6 ϕ 10	6 ϕ 10	0	80
			0.75	100
			1.5	120

As expected, Figure 21 shows similar results as the previous sets.

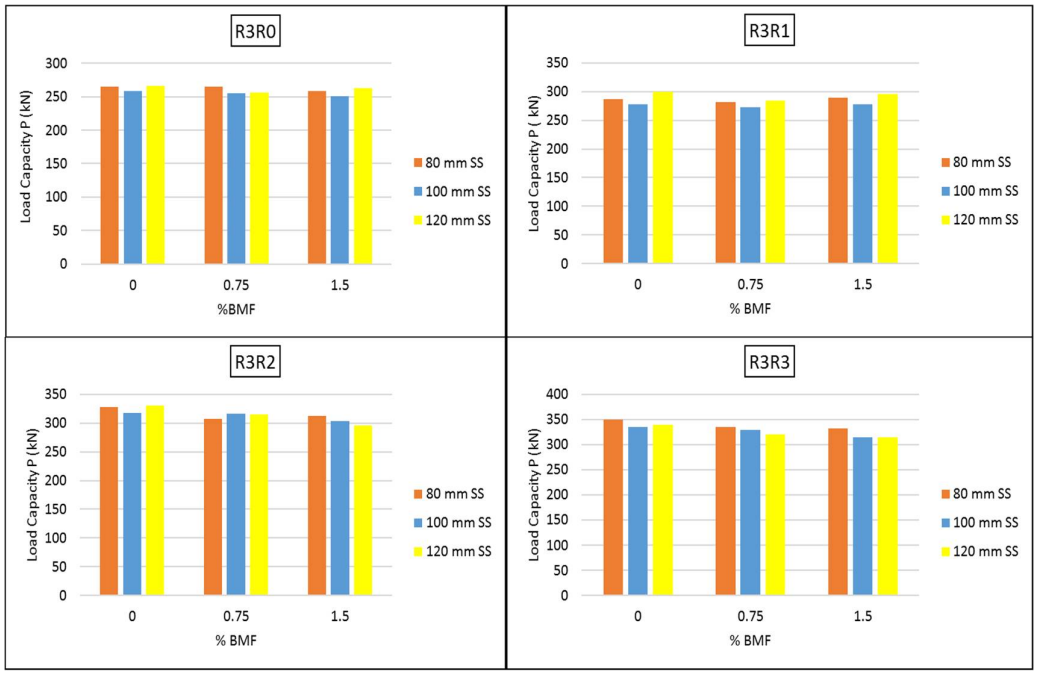

Figure 21: Load capacity for different stirrups spacing and BMF percentages for R3 group

6.3 Effect Bottom Reinforcement

In this section, four different bottom reinforcement ratios were investigated to study the effect of bottom reinforcement ratio on the (P) values. The studied ratios were 0.6 r_{fb}, 1 r_{fb}, 1.8 r_{fb} and 2.8 r_{fb}. The model was divided into sets based on the BMF, i.e., each set has same the BMF volume fraction with different values of other parameters. In each set, 48 beams were modeled.

6.3.1 Beams with $V_{f,BMF}$ = 0%

This set was modeled to have $V_{f,BMF}$ = 0% with different values of the other parameters. The effect of increasing the bottom reinforcement is shown in Figure 22. As shown in Figure 22, it is clear that increasing the bottom reinforcement along all levels of top

reinforcement had almost linear increment effect on all the ultimate moments of the modeled beams. The maximum rate of increment was 23% when the bottom reinforcement increased to R2. This is happened because bottom reinforcement R2 has over-reinforcement ratio.

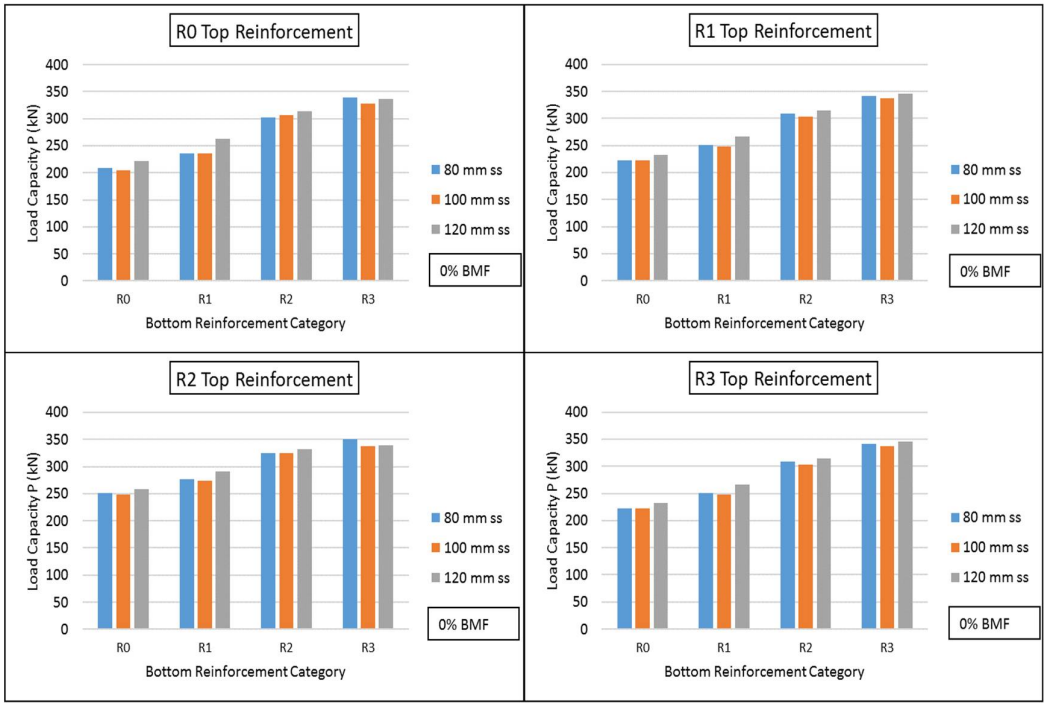

Figure 22: Effect of bottom reinforcement for $V_{f,BMF}$ = 0% set

6.3.2 Beams with $V_{f,BMF}$ = 0.75%

The set that has $V_{f,BMF}$ = 0.75% were modeled with the similar concept of 0% BMF set. As shown in Figure 23, the rate of increment in this set is equal to 26% which is higher than the $V_{f,BMF}$ = 0% set.

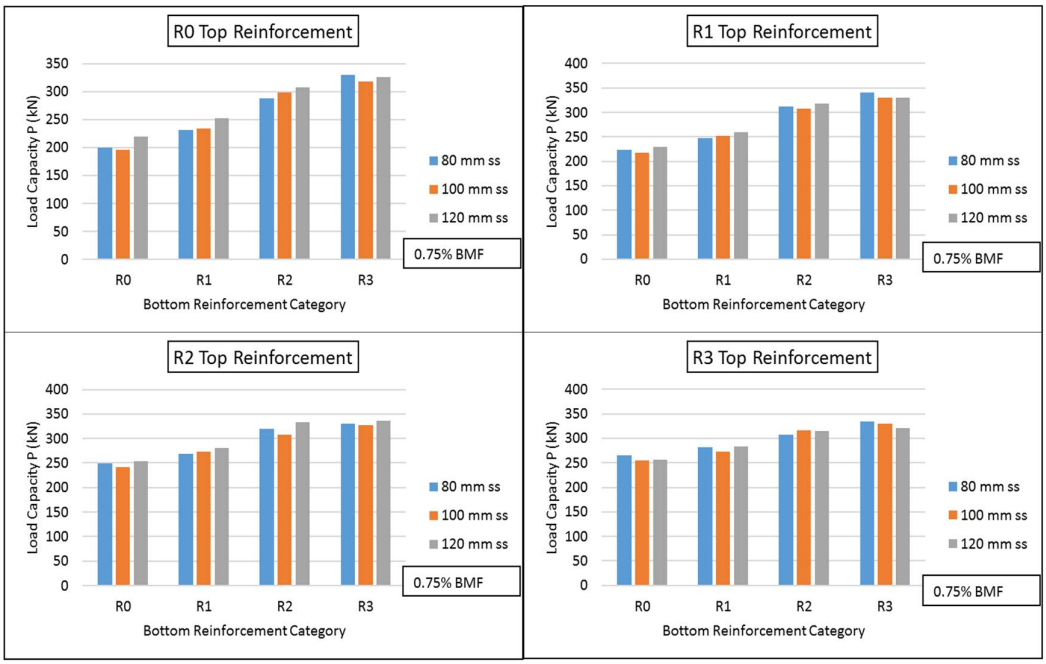

Figure 23: Effect of increasing bottom reinforcement for $V_{f,BMF}$ = 0.75% set

6.3.3 Beams with $V_{f,BMF}$ = 1.5%

The set that has $V_{f,BMF}$ = 1.5% were modeled with the similar concept of the 0% BMF set. As shown in Figure 24, the rate of increment is not increasing more that 26% which is the same rate of increment obtained from $V_{f,BMF}$ = 0.75%.

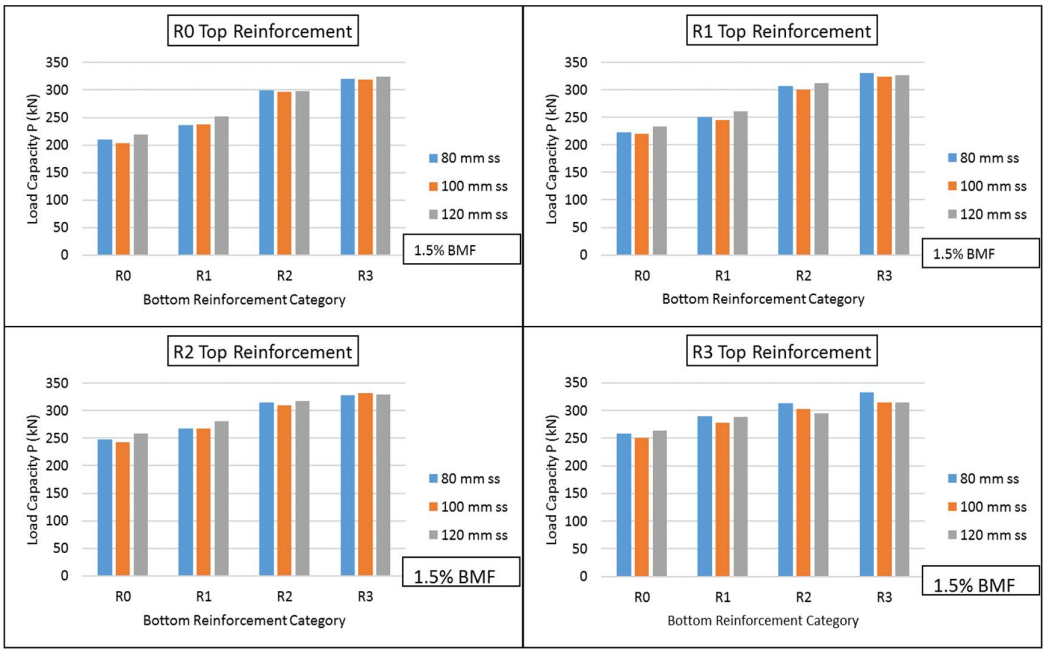

Figure 24: Effect of increasing bottom reinforcement for $V_{f,BMF}$ = 1.5% set

6.4 The Moment Redistribution

The moment redistribution of the continuous beams was investigated through the effect of three parameters namely, BMF volume fraction, stirrups spacing, and longitudinal reinforcement ratios. The first two parameters were studied as a combination to investigate if there is an effect of combining both parameters on the moment redistribution, while the third parameter was studied individually.

6.4.1 Forces and Moments Calculations

As mentioned earlier, three nodes were added at the supports in the FE model to record the reaction values at each loading step. The recorded reactions have been used in the calculation of the actual bending moments. In addition, the maximum applied load (P) before failure was recorded for each beam. The actual moments at the critical sections can be calculated from the following formulas:

Mid-span Moment = R_A x $\left(\frac{L}{2}\right)$ (9)

Middle Support Moment = $\left(\mathrm{P}\ \mathrm{x}\ \left(\frac{L}{2}\right)\right) - R_A\ \mathrm{x}\ \mathrm{L}$ (10)

Where:

R_A is the actual end reaction, L is the span length, P is the maximum applied load.

The elastic bending moments at the critical sections for the two spans beams can be calculated as:

$M_{mid\text{-}span} = 0.156 \text{ x P x L}$ (11)

$M_{middle\text{-}support} = 0.188 \text{ x P x L}$ (12)

The distribution of the moments is shown in Figure 25.

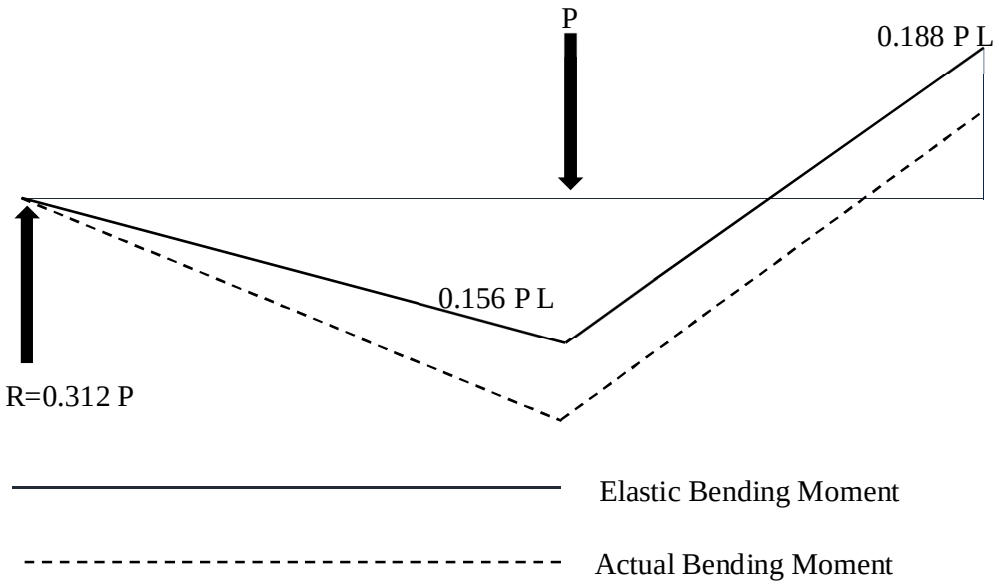

Figure 25: Elastic and actual bending moments

The moment redistribution percentages can be calculated from the following formula:

% Moment Redistribution = $(\frac{M_{actual} - M_{elastic}}{M_{actual}})$ x 100. (13)

Where:

$M_{elastic}$ and M_{actual} are the elastic and actual moments, respectively.

6.4.2 Effect of BMF and Stirrups Spacing

In this section, two main parameters were investigated; BMF and stirrups spacing. All modeled beams in this section were analyzed by dividing the beams into four sets based on the top reinforcement ratio. Each set had similar top reinforcement ratios with different values of other parameters. In each set, 36 beams were modeled.

6.4.3 Top Reinforcement (R0)

All the modeled beams in this set had a similar top reinforcement ratio and different values for the bottom reinforcement ratio, BMF and the stirrups spacing.

The effect of BMF and stirrups spacing on the moment redistribution is shown in Figure 26. In Figure 26, it was found that the effect of BMF is more noticeable than the effect of stirrups spacing such the 20% increment that was observed when 1.5% of BMF is added in R0R0 (120 mm stirrups spacing) beams. However, there was no clear trend on the relation between the stirrups spacing and the moment redistribution. This is because the main role of stirrups is to resist the shear forces and they are not contributing to the flexural behavior. On the other hand, an increment on the moment redistribution was observed with increasing the bottom reinforcement regardless of the remaining parameters because as the bottom reinforcement increases, the flexural strength will increase and will be able carry more loads. The effect of reinforcement ratios on the moment redistribution will be discussed in section 6.5.

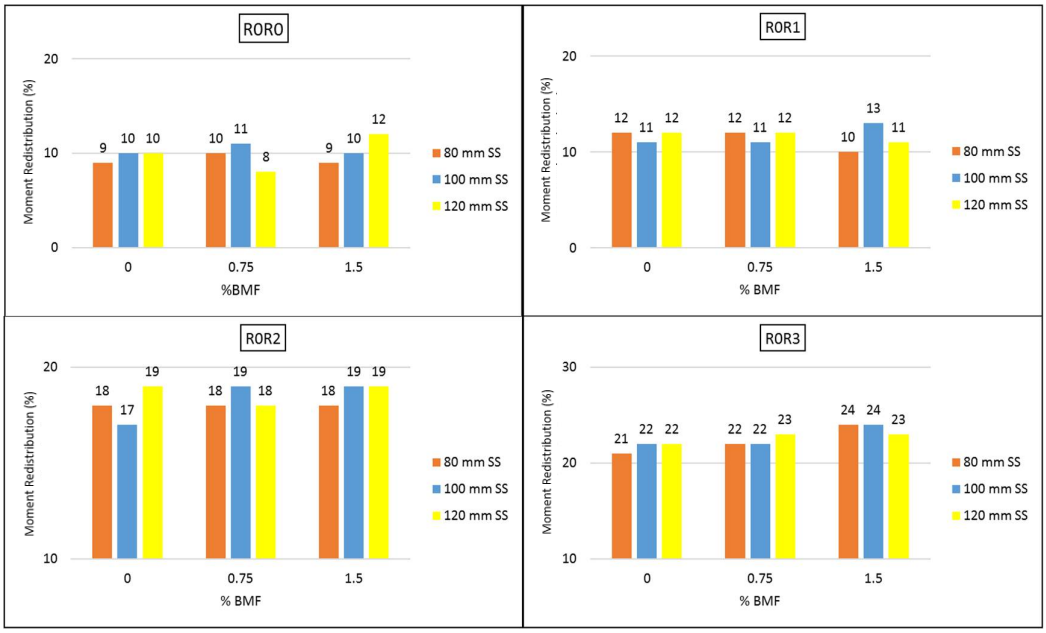

Figure 26: Moment redistribution for different stirrups spacing and BMF percentages for R0 group

6.4.4 Top Reinforcement (R1)

The set that has R1 as top reinforcement was modeled similar to R0 set. As shown in Figure 27, this set has experienced a significant reduction in the moment redistribution in all beams compared to the R0 set. It is known that when the top reinforcement increased, the stiffness will increase, therefore, this reduction in the moment redistribution can be attributed to the stiffness of the top reinforcement. The results showed also close values of moment redistribution with different stirrups spacing. However, a better moment redistribution values were noticed with the addition of BMF, except the beams belong to R1R0 has higher stiffness in the top. The maximum increment was 44% which is corresponding to 1.5% BMF R1R1 (120 mm stirrups spacing)

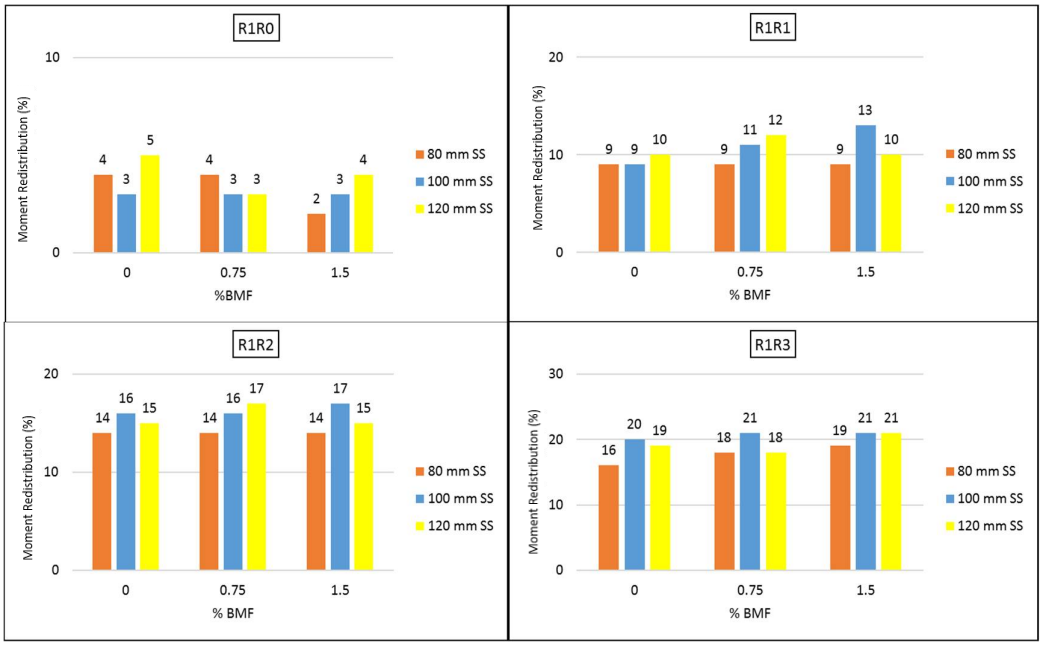

Figure 27: Moment redistribution for different stirrups spacing and BMF percentages for R1 group

6.4.5 Top Reinforcement (R2)

The set that has R2 as top reinforcement was modeled similar to R0 set. As shown in Figure 28, this set has experienced more reduction in the moment redistribution compared to R0, R1 sets. The values of the moment redistribution had a sudden jump after R2R0 and R2R1 beams, which is expected due to the arrangement of the longitudinal reinforcement and the tension failure that occurred in both. For R2R2 and R2R3 beams, the results showed an insignificant effect of the stirrups spacing, while it showed a clear improvement in the moment redistribution with the addition of the BMF. The maximum increment in the moment redistribution for this set was observed in R2R3 with120 mm stirrups spacing beams when 1.5% volume fraction is added.

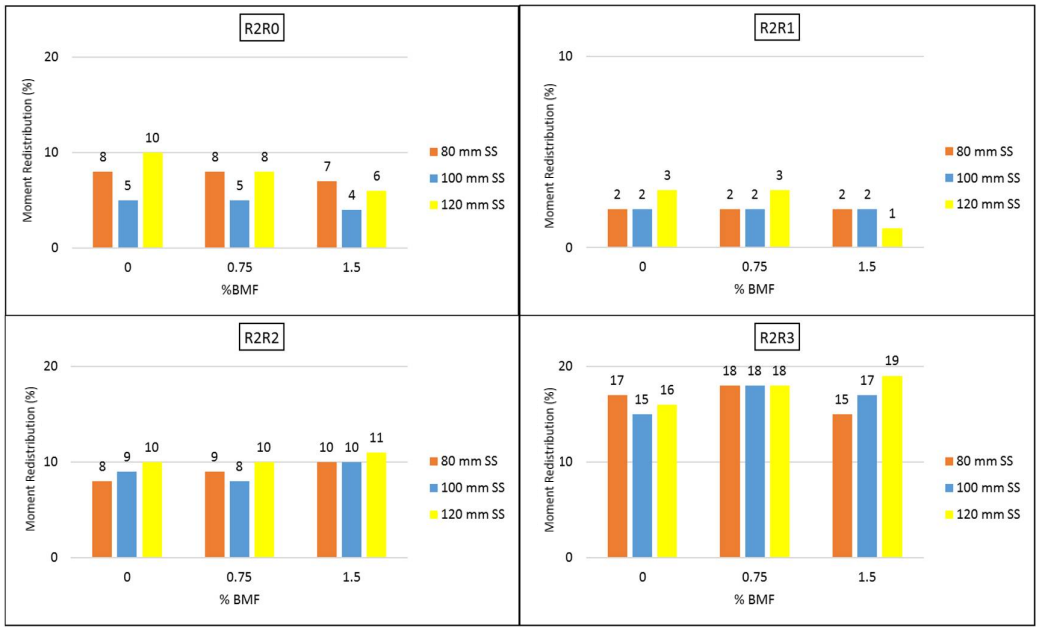

Figure 28: Moment redistribution for different stirrups spacing and BMF percentages for R2 group

6.4.6 Top Reinforcement (R3)

The set that has R3 as top reinforcement was modeled similar to R0 set. As shown in Figure 29, this set has experienced more reduction in the moment redistribution compared to R0, R1, R2 sets. The values of the moment redistribution are the highest in in the R3R3 beams due to the arrangement of the longitudinal reinforcement. In R3R3 beams, the results showed an unclear trend in the relation between the stirrups spacing and moment redistribution, while it showed a significant improvement in the moment redistribution with the addition of the BMF. It was increased by 35% when 0.75% of BMF was added in the beams that belong to R3R3 and they have 120 mm stirrups spacing.

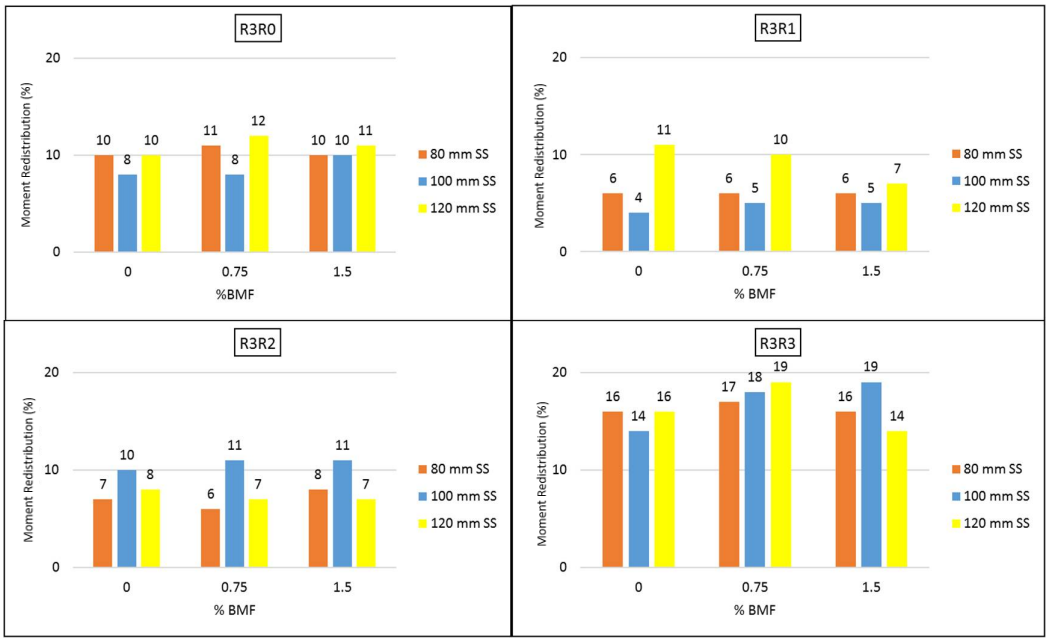

Figure 29: Moment redistribution for different stirrups spacing and BMF percentages for R3 group

6.5 Effect of Reinforcement Ratios

The effect of the longitudinal reinforcement ratios on the moment redistribution of BFRP continuous beams is presented in this section. The analysis was conducted by studying the effect of increasing the reinforcement ratio step-by-step from R0 to R3 for both the bottom and top reinforcement ratios.

6.5.1 Increasing Bottom Reinforcement from R0 to R1

This section aimed to study the effects of increasing the bottom reinforcement from R0 to R1, the modeled beams are listed in Table 12.

Table 12: Testing Matrix for the Studied Beams

From	To
R0R0	R0R1
R1R0	R1R1
R2R0	R2R1
R3R0	R3R1

As presented in Table11, in each top reinforcement category, the bottom reinforcement is increasing from R0 to R1. The results obtained are summarized in Figure 30.

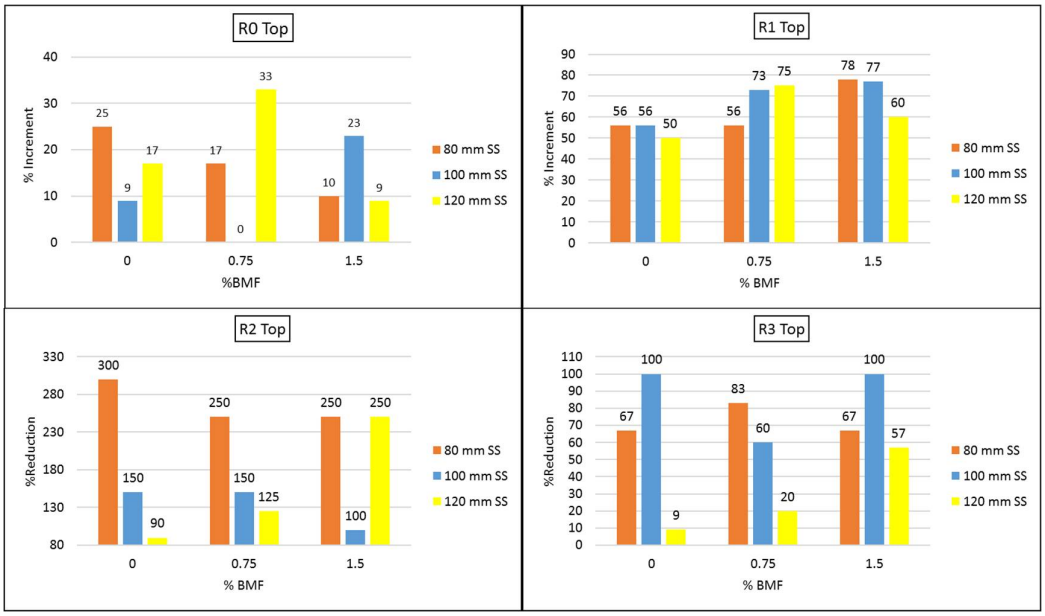

Figure 30: Moment redistribution for different stirrups spacing and BMF percentages for R1 bottom reinforcement

As shown in Figure 30, increasing the bottom reinforcement from R0 to R1 resulted in increasing the moment redistribution up to 77% for all beams except the beams that have R2 and R3 as top reinforcement, these beams have experienced a dramatic reduction in the moment redistribution. The reason behind this is believed to be the tension failure that occurred in R2R0, R3R0, and R3R1 beams and caused an inverse moment redistribution.

It was noticed that the rate of reduction and increment is not affected by the stirrups spacing and volume fraction of BMF. The results led to a conclusion that increasing the bottom reinforcement has a positive effect on the moment redistribution of the continuous beams.

6.5.2 Increasing Top Reinforcement from R0 to R1

This section aimed to study the effects of increasing the top reinforcement from R0 to R1, the simulated beams are listed in Table 13.

Table 13: Testing Matrix for the Studied Beams

From	To
R0R0	R1R0
R0R1	R1R1
R0R2	R1R2
R0R3	R1R3

As presented in Table 12, in each bottom reinforcement category, the top reinforcement is increasing from R0 to R1. The results obtained are summarized in Figure 31.

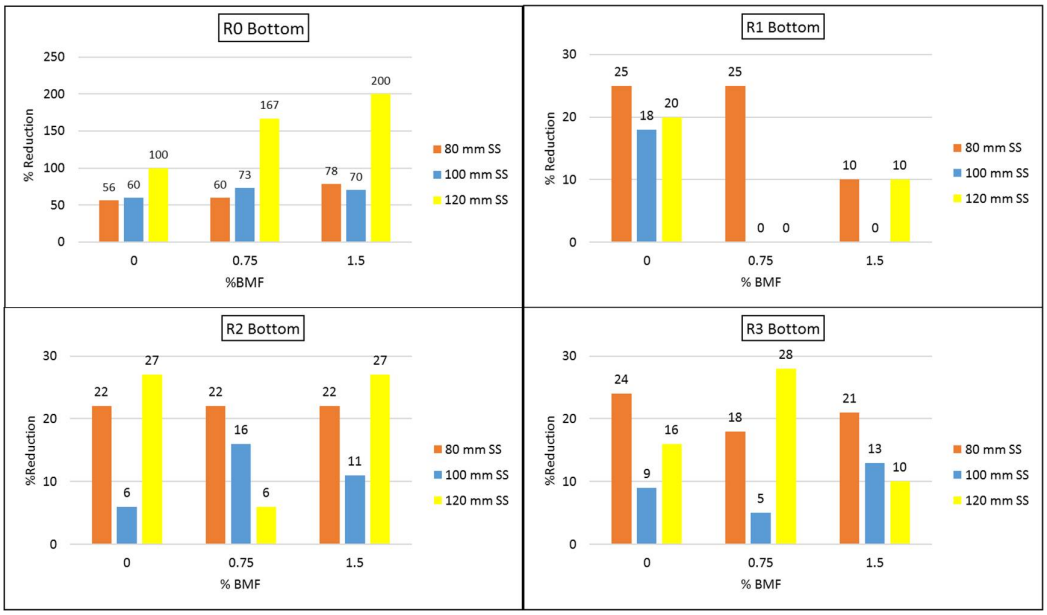

Figure 31: Moment redistribution for different stirrups spacing and BMF percentages for R1 top reinforcement

As shown in Figure 31, increasing the top reinforcement from R0 to R1 resulted in decreasing the moment redistribution in all beams. The rate of reduction was less with higher values of bottom reinforcement because the extra bars added in the bottom contribute in increasing the stiffness. It was observed that the rate of reduction is not affected by the stirrups spacing and BMF. A conclusion can be written that when increasing the top reinforcement ratio and keep the bottom reinforcement ratio constant will have a negative effect on the moment redistribution of the continuous beams.

6.5.3 Increasing Bottom Reinforcement from R1 to R2

In this section, the increment in the moment redistribution when the bottom reinforcement is increasing from R1 to R2 will be presented. The modeled beams covered in this analysis are listed in Table 14.

Table 14: Testing Matrix of the Studied Beams

From	To
R0R1	R0R2
R1R1	R1R2
R2R1	R2R2
R3R1	R3R2

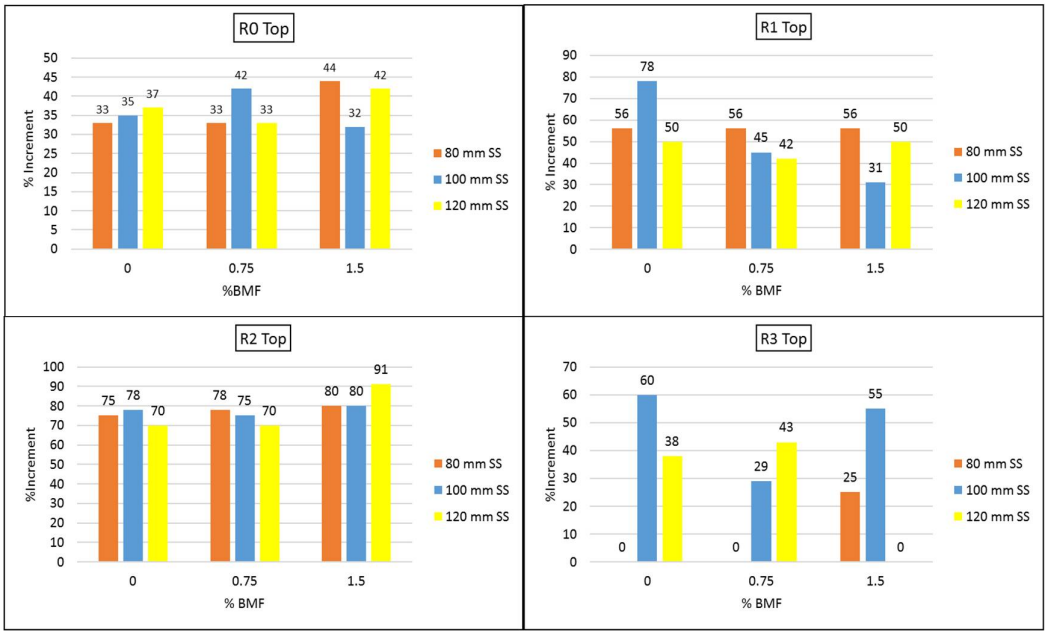

Figure 32: Moment redistribution for different stirrups spacing and BMF percentages for R2 bottom reinforcement

As shown in Figure 32, increasing the bottom reinforcement from R1 to R2 resulted in increasing the moment redistribution in all beams. The rate of increment was increasing with increasing the top reinforcement, except for R3 series. The rate of this series was less compared to the other series due to the tensile failure of the R3R0 beam. Again,

both BMF and stirrups spacing did not show clear a trend with the moment redistribution.

6.5.4 Increasing Top Reinforcement from R1 to R2

In this section, the change in the moment redistribution when the top reinforcement is increasing from R1 to R2 will be presented. The modeled beams covered in this analysis are listed in Table 15.

Table 15: Testing Matrix of the Studied Beams

From	To
R1R0	R2R0
R1R1	R2R1
R1R2	R2R2
R1R3	R2R3

The results obtained are summarized in Figure 33.

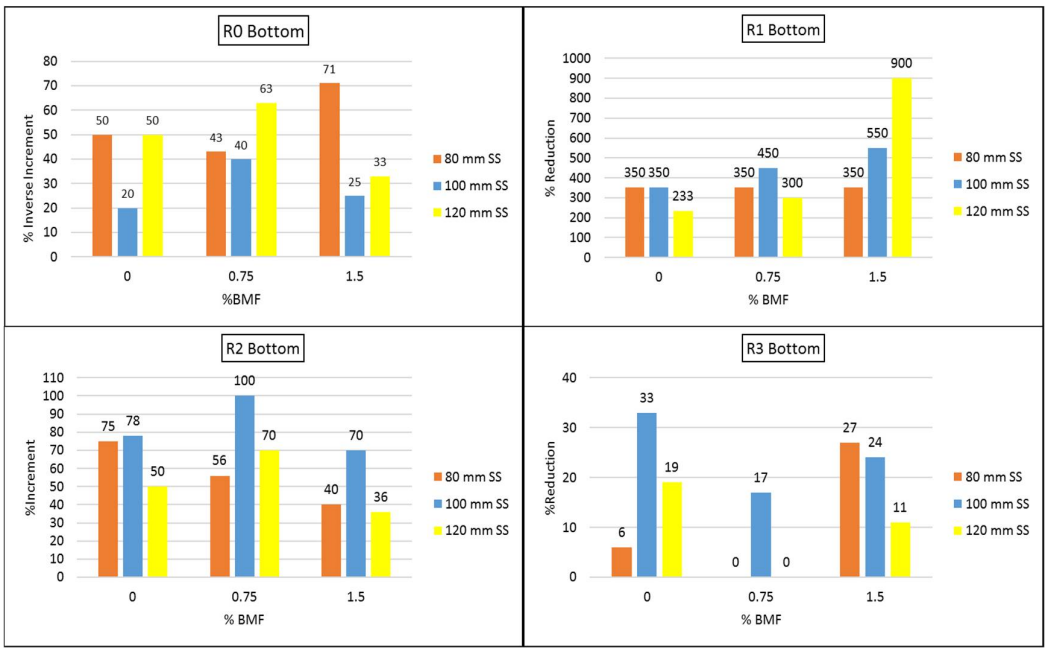

Figure 33: Moment redistribution for different stirrups spacing and BMF percentages for R2 top reinforcement

For the first series, where R1R0 beams were increased to R2R0, the beams failure mode was changed from compression to tension failure. Hence, the rate of increment in this series is described in the tensile behavior mode, where the moment is transferring from sagging to hogging support sections. For the second series, where R1R1 beams were increased to R2R1, the beams moment redistribution had dramatic reduction due to the difference in the stiffness between the top parts of R1R1 and R2R1 beams. A positive increment in the moment redistribution occurred for the third series, where the beam's top reinforcement was increasing from R1 to R2. There was a reduction in the moment redistribution for the fourth series, where beam's reinforcement was increased from

R1R3 to R2R3. This reduction took place due to the top stiffness was increased to an over reinforced section.

6.5.5 Increasing Bottom Reinforcement from R2 to R3

The aim of this section is to study the effects of increasing the bottom reinforcement from R2 to R3, the modeled beams are listed in Table 16.

Table 16: Testing Matrix of the Studied Beams

From	To
R0R2	R0R3
R1R2	R1R3
R2R2	R2R3
R3R2	R3R3

The results obtained are summarized in Figure 34.

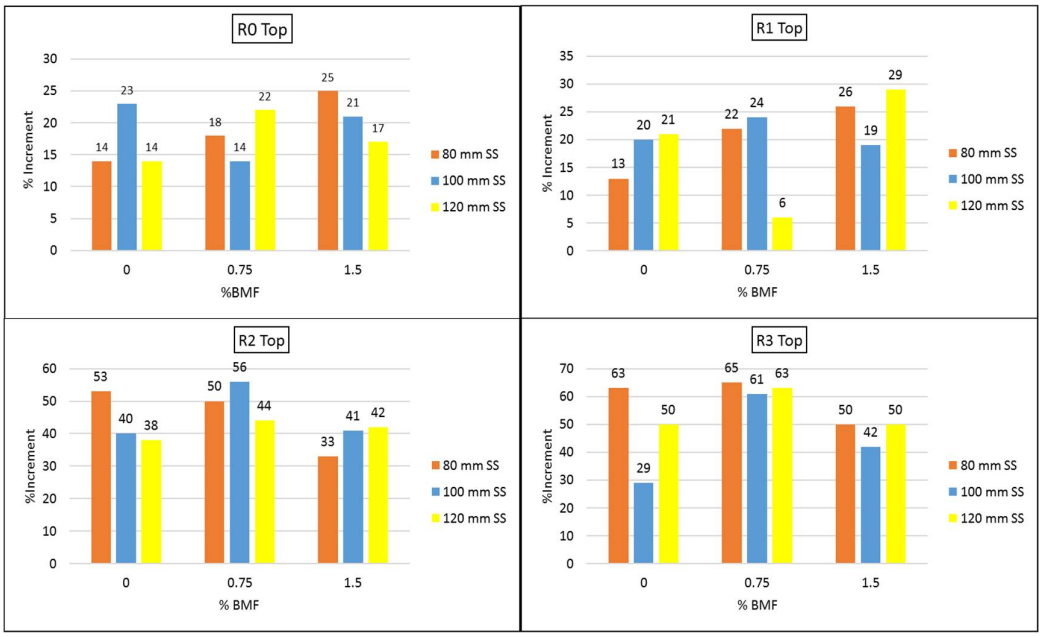

Figure 34: Moment redistribution for different stirrups spacing and BMF percentages for R3 bottom reinforcement

As shown in Figure 34, moment redistribution is increasing with increasing the bottom reinforcement from R2 to R3 for all values of top reinforcement. BMF and stirrups spacing parameters did not show any correlation with the moment redistribution.

6.5.6 Increasing Top Reinforcement from R2 to R3

The aim of this section is to study the effects of increasing the top reinforcement from R2 to R3, the simulated beams are listed in Table 17.

Table 17: Testing Matrix of The Studied Beams

From	To
R2R0	R3R0
R2R1	R3R1
R2R2	R3R2
R2R3	R3R3

The results obtained are summarized in Figure 35.

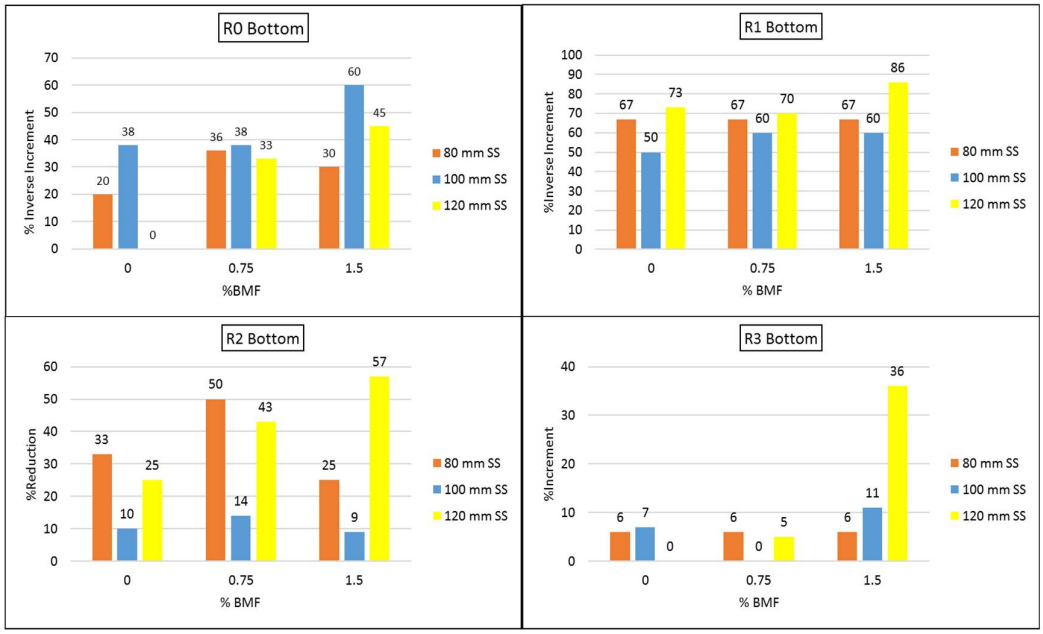

Figure 35:Moment redistribution for different stirrups spacing and BMF percentages for R3 top reinforcement

For both first and second series, where R2R0 and R2R1 beams were increased to R3R0 and R3R1, respectively, the beams failure mode was changed from compression to tension failure. Hence, the rate of increment in this series is described in the tensile behavior mode, where the moment is transferring from sagging to hogging sections. For the third series, the beams have experienced a reduction in the moment redistribution due to the increase in the top stiffness. The fourth series showed that increasing the top reinforcement in R2R3 beams will have very limited effect on the moment redistribution because both sections are over-reinforced. Again, it can be concluded that the effective moment redistribution occurs in the beams that have bottom reinforcement equal to or higher that the top reinforcement.

6.6 Statistical Analysis of the Results

A multiple linear regression analysis was performed on the moment redistribution results extracted from FE model. The analysis was performed using Minitab software. The relationship describing the multiple linear regression is shown in equation 13:

$$Y = \beta_o + \beta_1 x_1 + \beta_2 x_2 + \beta_3 x_3 \quad (13)$$

Where Y represents the response variable, x1, x2, x3 represent the predictor variables, and β_o, β_1, β_2 and β_3 represent the regression coefficients. The regression coefficients were estimated by the curve fitting analysis.

Six groups are used to derive the proposed model for the moment redistribution as:

1. Beams that have R0 top reinforcement.
2. Beams that have R1 top reinforcement.
3. Beams that have R2 top reinforcement.
4. Beams that have R3 top reinforcement.
5. Combination of beams 1, 2, 3 and 4 including the outliers.
6. Combination of beams 1, 2, 3 and 4 excluding the outliers.

For all groups, the proposed model is a function of volume of fraction of BMF, stirrups spacing, and reinforcement ratios.

6.6.1 Top Reinforcement (R0)

In this part, the regression was performed on all the beams that have R0 as top reinforcement. The results obtained are summarized in Table 18 and Figure 36.

Table 18: Regression Coefficients of the Studied Beams

Coefficient	Value
Intercept	4.78
BMF	0.5
Spacing	0.025
Bottom Reinforcement	0.03522

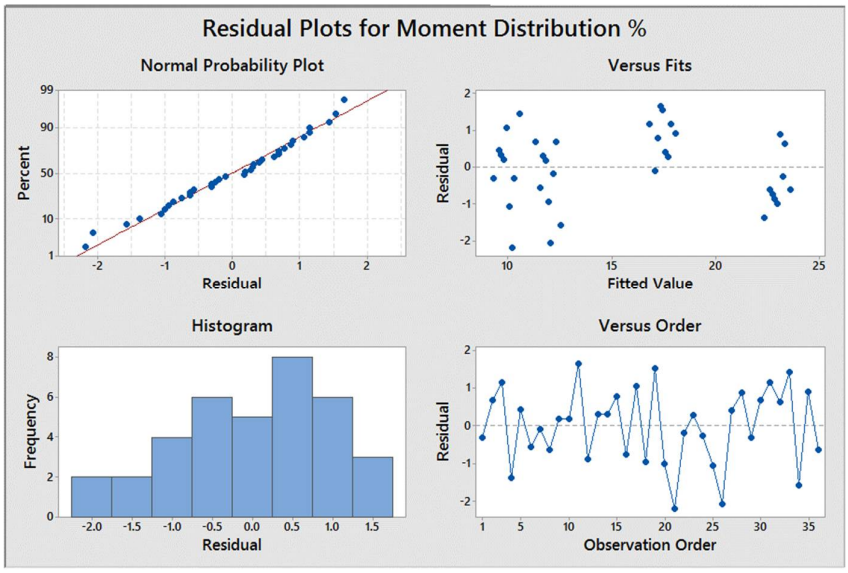

Figure 36: Residual plot for the moment redistribution of R0 set

The regression equation for this group can be expressed as shown in equation (14):

$$\%MR = 4.78 + 0.5\,FC\% + 0.0125\,stirrups\ spacing + 0.0352\,bottom\ reinforcement \quad (14)$$

The mean square of the error which is variance is equal to 1.072 which is adequate for the multiple linear regression. R^2 is equal to 96.14 % which means that the predicted model is covering 96.14% of the provided data which means highly correlated. From the normal probability plot, residual is plotted versus percent and it is shown that it is linear relation which means that the data are perfectly normally distributed in each level of predictors. From the histogram, it is noticed that the histogram is perfectly drawn which means that observations are normally distributed in each level of predictors. From residual versus fitted value diagram, it is shown that the points are randomly distributed around 0 line which indicates the assumption of linear relationship is valid. Also, the residual roughly from 0 lines which means the variance of the error is equal.

6.6.2 Top Reinforcement (R1)

In this section, the analysis of the beams that have R1 top reinforcement is presented. The results obtained are summarized in Table 19 and Figure 37.

Table 19: Regression Coefficients of the Studied Beams

Coefficient	Value
Intercept	-1.83
BMF	0.389
Spacing	0.0354
Bottom Reinforcement	0.03871

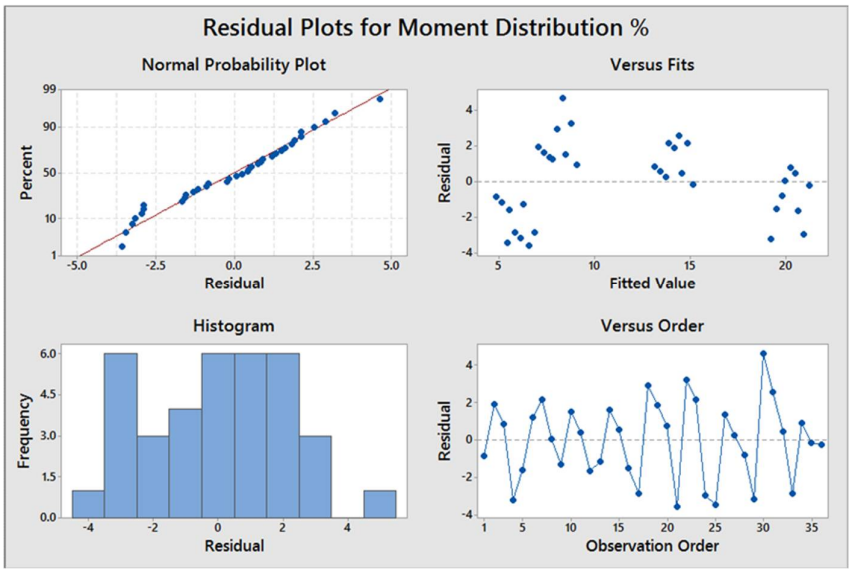

Figure 37: Residual plot for the moment redistribution of R1 set

The regression equation for this group can be expressed in equation 15:

$$\%MR = -1.83 + 0.389\ FC\% + 0.0354\ stirrups\ spacing + 0.03871\ bottom\ reinforcement \quad (15)$$

The variance is equal to 4.89 which is higher than the previous section. R^2 is equal to 86.81 % which means moderately correlated. R^2 in this group is less than the previous group due to the dramatic reduction in the moment redistribution in R1R0 beams compared to the other beams in the same group which is shown in normality plot that the first point is away from the fitting line. The negative value of the intercept can be interpreted as a reduction on the moment redistribution as discussed in section 6.4.4 which showed that moment redistribution will be decreased if the top reinforcement ratio increases to balanced reinforcement ratio. From the histogram, it is noticed that the histogram is drawn with accepted normality which means that observations normality level is accepted. From the residual versus fitted value diagram, it is shown that the points are randomly distributed around 0 line which indicates the assumption

of linear relationship is valid. Also, the residual roughly from 0 lines which means the variance of the error is equal.

6.6.3 Top Reinforcement (R2)

The analysis of the beams that have R2 top reinforcement is presented in this section. The results obtained are summarized in Table 20 and Figure 38.

Table 20: Regression Coefficients of the Studied Beams

Coefficient	Value
Intercept	-1.94
BMF	-0.056
Spacing	0.0208
Bottom Reinforcement	0.03342

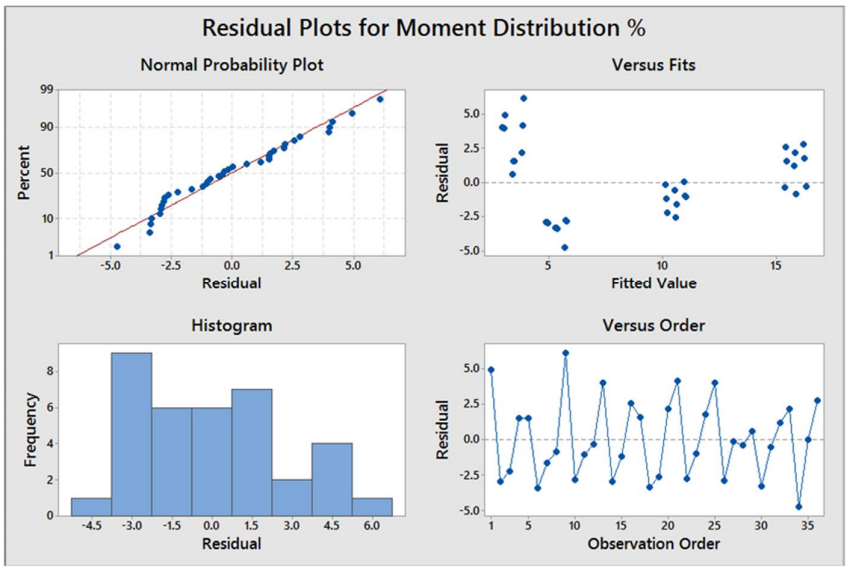

Figure 38: Residual plot for the moment redistribution of R2 set

The regression equation for this group can be expressed in equation 16:

$$\%MR = -1.94 - 0.056\ FC\% + 0.0208\ stirrups\ spacing + 0.03342\ bottom\ reinforcement \quad (16)$$

The variance is equal to 8.21 which is higher than the previous two sections. R^2 is equal to 74.04% which means slightly correlated. R^2 is low in this group due to the inverse moment redistribution in R2R0 beams. From the normal probability plot, it is shown that many outliers in the best fit line which is affecting the linearity of the model. From the histogram, it is noticed that the histogram is drawn with less linearity. From residual versus fitted value diagram, it is shown that the points are not perfectly randomly distributed around 0 line which indicates that it has a less linear model.

As expected, the intercept for this group was less than the previous groups because in this group there are R2R0 and R2R1 in which both are causing a reduction in the moment redistribution.

6.6.4 R3 Top Reinforcement

The analysis of the beams that have R3 top reinforcement is presented in this section. The results obtained are summarized in Table 21 and Figure 39.

Table 21: Regression Coefficients of the Studied Beams

Coefficient	Value
Intercept	2.12
BMF	0.278
Spacing	0.0292
Bottom Reinforcement	0.01920

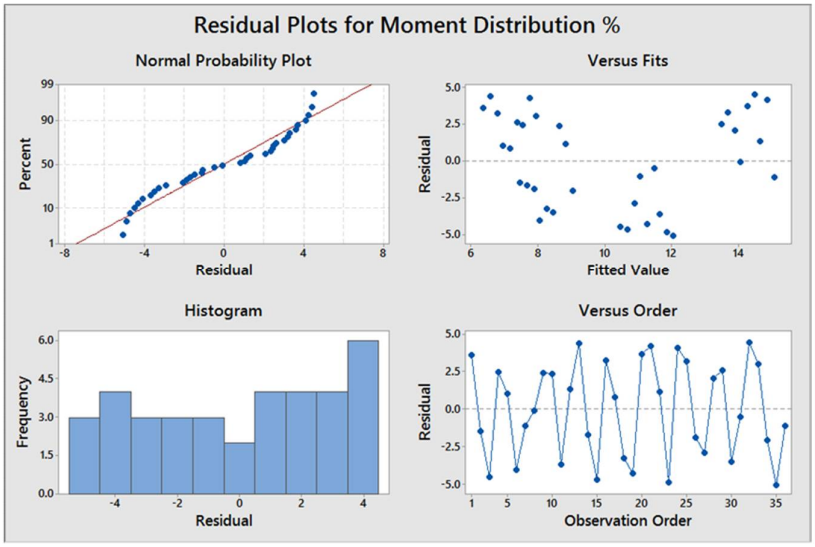

Figure 39: Residual plot for the moment redistribution of R3 set

The regression equation for this group is shown in equation 17:

$$\%MR = -2.12 + 0.278\ FC\% + 0.0292\ SS + 0.0192\ bottom\ reinforcement \quad (17)$$

As expected, the regression of this group was the lowest in the linearity properties. The standard deviation is equal to 11. R^2 is equal to 39.73 % which means that predicted model is covering only 39.73 % of the provided data which means poorly correlated due to the inverse moment redistribution in R3R0, R3R1 beams, and opposite arrangement of the reinforcement in R3R2 beams, i.e., top stiffness is higher than bottom stiffness.

The positive value of the intercept can be interpreted as the bottom reinforcement increase, the inverse %MR will decrease. From the normal probability plot, it is shown that most of the points are outliers which is affecting the linearity of the model. From the histogram, it is noticed that the histogram is drawn with no linearity. From residual versus fitted value diagram, it is shown that the points are not randomly distributed around 0 line which indicates that it has poor linear model.

6.6.5 Combination with Outliers

In this section, all values have been combined to generate a linear model, the coefficients obtained are shown in Table 22 and Figure 40.

Table 22: Regression Coefficients of the Studied Beams

Coefficient	Value
Intercept	4.28
BMF	0.278
Spacing	0.0245
Top Reinforcement	-0.0134
Bottom Reinforcement	0.03164

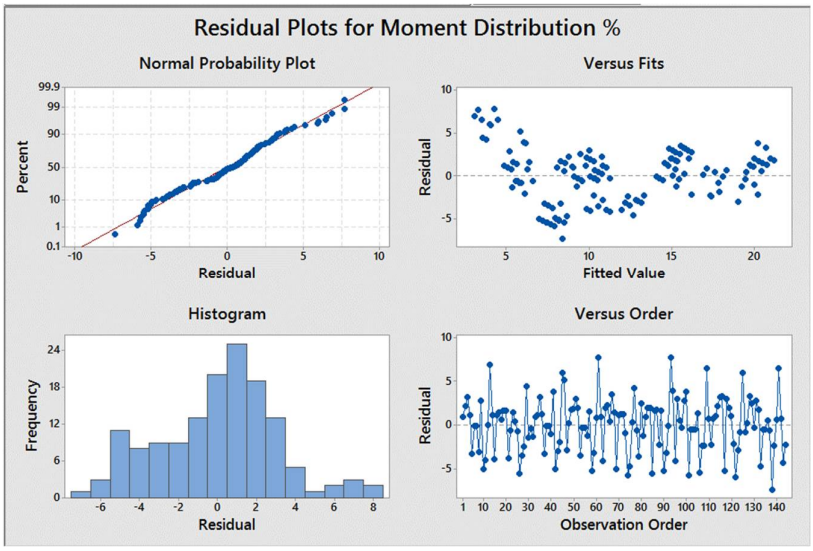

Figure 40: Residual plot for the moment redistribution of combination with outliers

The regression equation for this group is shown in equation (18):

$$\%MR = 4.28 + 0.278\,\%FC + 0.0245\,SS - 0.01343\,top\ reinforcement + 0.03164\,bottom\ reinforcemnt \quad (18)$$

The R^2 value obtained in this model is 71.71% which is poorly correlated. Standard deviation is equal to 9.78. This is because of the reasons mentioned in the previous sections.

6.6.6 Combination Excluding the Outliers

In this section, R2R0, R3R0, and R3R1 have been eliminated to generate a better model, the results obtained are shown in Table 23 and Figure 41.

Table 23: Regression Coefficients of the Studied Beams

Coefficient	Value
Intercept	3.72
BMF	0.444
Spacing	0.0212
Top Reinforcement	-0.0250
Bottom Reinforcement	0.04102

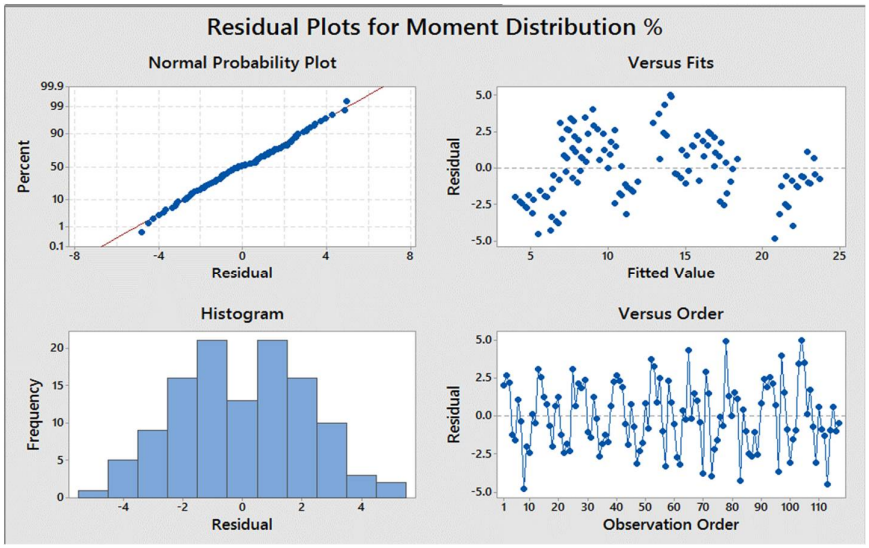

Figure 41: Residual plot for the moment redistribution of combination without outliers

The regression equation for this group is shown in equation (19):

$$\%MR = 3.72 + 0.444\,\%FC + 0.0212\,SS - 0.02505\,top\ reinforcement + 0.04102\,bottom\ reinforcemnt \quad (19)$$

This model has R^2 value as 87.28% which is moderately correlated. Standard deviation is equal to 4.87 which is less than the value obtained in section 4.7.2. From the probability plot, it is clearly shown that the model is linear except for the two outliers point which related to R1R0 and R2R1. From the histogram, it is clearly shown that the histogram is drawn with accepted normality which means that observations normally level is accepted. From residual versus fitted value diagram, it is shown that the points are randomly distributed around 0 line which indicates the assumption of linear relationship is valid. Also, the residual roughly from 0 lines which means the variance of the error is equal.

6.6.7 Validating the Regression Equation

In this section, a new FE model which was not part of the previously studied matrix will be used to validate the regression equation 19. The model that have been chosen is shown in Table 24.

Table 24: FEM Model to Validate the Regression Equation

Bottom Reinforcement	Top Reinforcement	Stirrups Spacing (mm)	%BMF	Transverse Reinforcement	Longitudinal Reinforcement
3 ϕ 10	4 ϕ 10	110	0.75	Steel	BFRP-Ribbed Bar

A comparison between FEA and the regression equation is shown in Table 24. From Table 25, the percentage error is 3.6% which verify the accuracy of the regression equation.

Table 25: Model Moment Redistribution Result and Percentage Error

P (kN)	End Reaction (kN)	Moment Redistribution (FEA)	Moment Redistribution (Regression)	%Error
320.5	114	13.9	13.4	3.6

CHAPTER 7: SUMMARY, CONCLUSIONS AND RECOMMENDATIONS

7.1 Summary

This study has investigated the moment redistribution in the beams reinforced with BFRP bars using finite element method (FEM). The key parameters considered in this study were: volume fraction of BMF, stirrups spacing and longitudinal reinforcement ratios. The results showed a significant improvement in the moment redistribution when both top and bottom reinforcement are over-reinforced. Also, adding BMF to the concrete mix showed a positive effect in improving the moment redistribution while, the moment redistribution did not show clear trend with the stirrups spacing.

7.2 Conclusions

The following conclusion can be drawn from this study:

1. FRC stress-strain diagram used in this study was accurately predicted using numerical equation and it was verified with the experimental stress-strain diagram and good agreement was achieved.
2. The proposed FE model was verified against experimental results of FRC continuous beams obtained from Qatar University structural lab.
3. Volume fraction of BMF and stirrups spacing has negligible effect on the maximum applied load (P). This is because both parameters have no effect on the compressive flexural strength.
4. Beam's (P) values is increasing with increasing the bottom reinforcement ratio.
5. The effect of the bottom reinforcement ratio on the moment redistribution was more pronounced than the top reinforcement ratio. This is because the bottom reinforcement has a significant effect on the compressive strength.
6. Moment redistribution was effectively observed on the beams that have top reinforcement ratio equal or less than the bottom reinforcement ratio.

7. The ratio between bottom reinforcement to top reinforcement should be higher than 0.3 in order not to change the failure mode.
8. Linear regression model that can predict the moment redistribution in FRC continuous beams reinforced with BFRP bars was generated with high accuracy.

7.3 Recommendations for Future Work

For future work related to the moment redistribution on the BFRP beams, it is recommended to conduct more experiments on the performance of BFRP beams with different loading configuration and other types of cross-sections such as, T section. Furthermore, it is necessary to model the beams with different types of fibers, different compressive strengths, and more than two spans.

REFERENCES

ACI Committee 440. (2015). Guide for the Design and Construction of Structural Concrete Reinforced with Fiber-Reinforced Polymer (FRP) Bars: ACI 440.1R-15. In. Farmington Hills, MI: American Concrete Institute.

Adam, M. A., Said, M., Mahmoud, A. A., & Shanour, A. S. (2015). Analytical and experimental flexural behavior of concrete beams reinforced with glass fiber reinforced polymers bars. *Construction and Building Materials, 84*, 354-366.

Adhikari, S. (2013). *Mechanical and structural characterization of mini-bar reinforced concrete beams.* University of Akron,

Ayub, T., & Khan, S. U. (2017). *Finite element modelling of FRC beams containing PVA and Basalt fibres: A comparative study.* Paper presented at the AIP Conference Proceedings.

Ayub, T., Khan, S. U., & Shafiq, N. (2018). Flexural Modelling and Finite Element Analysis of FRC Beams Reinforced with PVA and Basalt Fibres and Their Validation. *Advances in Civil Engineering, 2018*.

Ayub, T., Shafiq, N., & Nuruddin, M. F. (2014). Effect of chopped basalt fibers on the mechanical properties and microstructure of high performance fiber reinforced concrete. *Advances in Materials Science and Engineering, 2014*.

Bagge, N., O'Connor, A., Elfgren, L., & Pedersen, C. (2014). Moment redistribution in RC beams–A study of the influence of longitudinal and transverse reinforcement ratios and concrete strength. *Engineering structures, 80*, 11-23.

Cai, J., Pan, J., & Zhou, X. (2017). Flexural behavior of basalt FRP reinforced ECC and concrete beams. *Construction and Building Materials, 142*, 423-430.

Carpinteri, A., Corrado, M., Paggi, M., & Mancini, G. (2009). New model for the analysis of size-scale effects on the ductility of reinforced concrete elements in bending. *Journal of engineering mechanics, 135*(3), 221-229.

CSA. (2012). S806-12 - Design and construction of building structures with fibre-reinforced polymers. In. Mississauga, Ontario, Canada: Canadian Standards Association.

Do Carmo, R., & Lopes, S. (2006). Required plastic rotation of RC beams. *Proceedings of the Institution of Civil Engineers-Structures and Buildings, 159*(2), 77-86.

El-Mogy, M., El-Ragaby, A., & El-Salakawy, E. (2010). Flexural behavior of continuous FRP-reinforced concrete beams. *Journal of Composites for Construction, 14*(6), 669-680.

El-Mogy, M., El-Ragaby, A., & El-Salakawy, E. (2011). Effect of transverse reinforcement on the flexural behavior of continuous concrete beams reinforced with FRP. *Journal of Composites for Construction, 15*(5), 672-681.

EN, B. (2004). Eurocode 2: Design of concrete structures Part 1-1–General rules and rules for buildings (including NA). *London: British Standards Institution*.

Ernst, G. C. (1958). *Moment and shear redistribution in two-span continuous reinforced concrete beams.* Paper presented at the Journal Proceedings.

Grace, N. F., Soliman, A., Abdel-Sayed, G., & Saleh, K. (1998). Behavior and ductility of simple and continuous FRP reinforced beams. *Journal of Composites for Construction, 2*(4), 186-194.

Gravina, R. J., & Smith, S. T. (2008). Flexural behaviour of indeterminate concrete beams reinforced with FRP bars. *Engineering Structures, 30*(9), 2370-2380.

Habeeb, M., & Ashour, A. F. (2008). Flexural behavior of continuous GFRP reinforced concrete beams. *Journal of Composites for Construction, 12*(2), 115-124.

High, C., Seliem, H. M., El-Safty, A., & Rizkalla, S. H. (2015). Use of basalt fibers for concrete structures. *Construction and Building Materials, 96*, 37-46.

Imjai, T., Guadagnini, M., & Pilakoutas, K. (2017). Bend strength of FRP bars: experimental investigation and bond modeling. *Journal of Materials in Civil Engineering, 29*(7), 04017024.

ISIS CANADA. (2007). Reinforcing Concrete Structures with Fibre Reinforced Polymers. In. Winnipeg, Manitoba, Canada: ISIS CANADA Corporation, The Canadian Network of Centres of Excellence on Intelligent Sensing for Innovative Structures.

Jason, L., Pijaudier-Cabot, G., Huerta, A., & Ghavamian, S. (2004). *Damage and plasticity for concrete behavior.* Paper presented at the European Congress on Computational Methods in Applied Sciences and Engineering.

Jędrzejczak, M., & Knauff, M. (2002). Redystrybucja momentów zginających w żelbetowych belkach ciągłych-zasady polskiej normy na tle Eurokodu. *Inżynieria i Budownictwo, 58*(8), 428-430.

Kara, I. F., & Ashour, A. F. (2013). Moment redistribution in continuous FRP reinforced concrete beams. *Construction and Building Materials, 49*, 939-948.

Kodur, V. K. R., & Campbell, T. (1996). Evaluation of moment redistribution in a two-span continuous prestressed concrete beam. *Structural Journal, 93*(6), 721-728.

Lin, C. H., & Chien, Y. M. (2000). Effect of section ductility on moment redistribution of continuous concrete beams. *Journal of the Chinese Institute of Engineers, 23*(2), 131-141.

Lopes, S., & Bernardo, L. (2003). Plastic rotation capacity of high-strength concrete beams. *Materials and Structures, 36*(1), 22-31.

Lou, T., Lopes, S. M., & Lopes, A. V. (2015). Neutral axis depth and moment redistribution in FRP and steel reinforced concrete continuous beams. *Composites Part B: Engineering, 70*, 44-52.

Metwally, I. M. (2017). Three-dimensional nonlinear finite element analysis of concrete deep beam reinforced with GFRP bars. *HBRC journal, 13*(1), 25-38.

Mostafa, A. A., & Razaqpur, A. G. (2017). Finite element model for predicting post delamination behaviour in FRP-retrofitted beams in flexure. *Construction and Building Materials, 131*, 195-204.

Park, R. L., Park, R., & Paulay, T. (1975). *Reinforced concrete structures*: John Wiley & Sons.

Patnaik, A., Miller, L., Adhikari, S., & Standal, P. C. (2013). Basalt FRP minibar reinforced concrete. *Fibre Concrete*, 12-13.

Pawłowski, D., & Szumigała, M. (2015). Flexural behaviour of full-scale basalt FRP RC beams–experimental and numerical studies. *Procedia Engineering, 108*, 518-525.

Piotr, D., & Krzysztof, K. (2017). Research in redistribution of bending moments in the beams of reinforced concrete early loaded. *Procedia Engineering, 172*, 883-890.

Rahman, S. H., Mahmoud, K., & El-Salakawy, E. (2016). Behavior of Glass Fiber–Reinforced Polymer Reinforced Concrete Continuous T-Beams. *Journal of Composites for Construction, 21*(2), 04016085.

Rahman, S. H., Mahmoud, K., & El-Salakawy, E. (2017). Moment redistribution in glass fiber reinforced polymer-reinforced concrete continuous beams subjected to unsymmetrical loading. *Engineering Structures, 150*, 562-572.

Razaqpur, A., & Mostofinejad, D. (1999). Experimental study of shear behavior of continuous beams reinforced with carbon fiber reinforced polymer. *Special Publication, 188*, 169-178.

Rjoub, M. (2006). Moment capacity of steel fiber reinforced concrete beams. *Journal of Engineering Sciences, 34*(2), 413-422.

Systèmes, D. (2013). Abaqus 6.14–Analysis Users's Guide: Volume IV: Elements. *Providence, Rhode Island*.

Tezuka, M., Ochiai, M., Tottori, S., & Sato, R. (1995). *Experimental study on moment redistribution of continuous beams reinforced or pretensioned with fiber reinforced plastic.* Paper presented at the RILEM PROCEEDINGS.